

A quantum algorithm for solving open system dynamics on quantum computers using noise

Juha Leppäkangas, Nicolas Vogt, Keith R. Fratus, Kirsten Bark, Jesse A. Vaitkus, Pascal Stadler, Jan-Michael Reiner, Sebastian Zanker, and Michael Marthaler
HQS Quantum Simulations GmbH, Rintheimer Str. 23, 76131 Karlsruhe, Germany

In this paper we present a quantum algorithm that uses noise as a resource. The goal of our quantum algorithm is the calculation of operator averages of an open quantum system evolving in time. Selected low-noise *system qubits* and noisy *bath qubits* represent the system and the bath of the open quantum system. All incoherent qubit noise can be mapped to bath spectral functions. The form of the spectral functions can be tuned digitally, allowing for the time evolution of a wide range of open-system models at finite temperature. We study the feasibility of this approach with a focus on the solution of the spin-boson model and assume intrinsic qubit noise that is dominated by damping and dephasing. We find that classes of open quantum systems exist where our algorithm performs very well, even with gate errors as high as 1%. In general the presented algorithm performs best if the system-bath interactions can be decomposed into native gates.

I. INTRODUCTION

Quantum computers promise a substantial speedup for solving certain types of numerical tasks, in particular the simulation of large quantum systems [1]. However, due to the large error rates and short coherence times of present quantum computers [2], only small examples have been demonstrated using digital quantum computing. For useful near-term applications, there is a need for current research to be focused on more efficiently exploiting noisy intermediate-scale quantum (NISQ) computers. In this paper we present a quantum algorithm which, in fact, utilizes typical noise in NISQ devices by incorporating it into the computation itself.

Models for open quantum systems [3, 4] (short, open-system models or OSM) have been developed for the study of a small number of degrees of freedom, the system, interacting with a large environment, the bath. Accordingly, the use of an open-system model is often called the system-bath approach. The idea is that certain dynamical or steady-state properties of the system can be the key to understanding the overall behavior of the full system-environment pair. The bath can be modeled with less accuracy, making the approach economic. One widely studied example is the energy transfer involved in photosynthesis [5], where the system is a finite number of local excitations (excitons) and the bath are the vibrational modes. The effect of the bath on the system is described by a spectral function and the effect strongly depends on its height and form [6]. The limit of a smooth spectral function (on the scale of the system-bath couplings) can be described by the well-known Lindblad or Bloch-Redfield master equation.

An open system is characterized by non-unitary time evolution. Therefore, a quantum algorithm that time evolves an open-system model on a quantum computer must implement this in some way. Non-unitary operations can be implemented by introducing additional qubits and measurements [7–18]. Most such approaches directly consider an open-system model that can be de-

scribed by a Lindblad master equation. Time evolution under a Lindblad master equation can be performed on a quantum computer using the same Trotterization approach known for closed quantum systems: the system is coupled to the external qubits at each Trotter step, which are measured and thus create non-unitary quantum operations. A technical challenge here is the reset of the external qubits after each Trotter step during the computation. This can be done, for example, with the help of qubit damping [11, 13, 14].

The most efficient way to implement non-unitary gates on NISQ computers is via noise utilization [11–15, 19–21]. By performing noise utilization, noise is no longer an impediment, but is rather a key component of the computation itself. Although digital quantum computers performing a Trotter time-evolution might involve many different gate operations, it is possible to describe the effect of noise in the form of a static Lindblad master equation operating on the time-evolved density matrix [22]. However, a limitation of noise-utilizing quantum algorithms so far has been that most previous work falls in the category of smooth spectral functions.

In this paper, we present a noise-utilizing algorithm that is designed to time-evolve open-system models with strongly structured spectral functions. In this approach, low and high noise qubits become the system and bath qubits, respectively. They represent the system and the bath of the open quantum system. Significant variations in qubit coherence times may appear in state-of-the-art quantum computers [23], and it is typically possible during calibration to make some qubits better at the expense of others, for example, to avoid frequency crowding of the good qubits. In our work, we use this to our advantage by using the lower quality qubits as bath qubits for mimicking the effect of a continuous spectral function. We give a detailed description of how the spectral function, as seen by the time-evolved system, can be made strongly structured, digitally tunable and to match to the open-system model of interest.

The performance of the proposed algorithm is stud-

ied through numerical simulation on conventional computers. In particular, we study the quality of the results of the algorithm for a spin coupled strongly to a broad bosonic mode as well as to a bosonic ohmic bath. Here, we establish a mapping between the open-system model and the noisy-algorithm model in the case of noiseless system-qubits. We also study the solution for an electron-transport model by representing it using a generalized spin-boson model. Here, we map also the system-qubit noise to the model spectral function. Our central finding is that the quantum algorithm performs best if the system-bath interactions can be decomposed into native gates, for instance the XX Ising interaction to variable Mølmer-Sørensen (MS) gate or the XX + YY interaction to variable iSWAP gate. The restriction to native gates can, however, be lifted for some open-system models.

The paper is structured as follows. In Sec. II, we introduce the concrete open system model whose noise-utilizing quantum algorithm will be presented in this paper. In Sec. III, we present the protocol of the bath mapping, *i.e.*, the mapping between an open-system model and a noisy-algorithm model. In Sec. IV, we go through three practical examples of solving the open-system dynamics. The examples were implemented using numerical simulations on conventional computers. Conclusions and discussion are given in Sec. V. Many important details of our approach are left to be presented in the Appendices. In Appendix A, we generalize the approach to also cover multi-spin systems. In Appendix B, we go through details of our model of noisy quantum computation. In Appendix C, we discuss principles of a quantum circuit optimization, which engineers effective Lindbladians to a useful form. In Appendix D, we quantify the main error sources and the error tradeoff in our approach. Finally, in Appendix E, we discuss how to map a fermionic open-system model to a spin-boson model.

II. OPEN-SYSTEM MODEL

While the plethora of physical phenomenon encountered in nature naturally correspond to a wide range of potential open system models, we focus here on one concrete model of a specific form. In particular, in its most general form, the open-system Hamiltonian we consider can be written

$$\hat{H}_0 = \hat{H}_S + \hat{H}_B + \hat{H}_C, \quad (1)$$

where \hat{H}_S is the Hamiltonian of the system, \hat{H}_B of the bath, and \hat{H}_C describes their coupling.

In this work, we explicitly consider problems that can be represented as a two-state system interacting with a

bosonic bath [6] by the so-called spin-boson model:

$$\hat{H}_S = \frac{\hbar\Delta}{2} \hat{\sigma}_z, \quad (2)$$

$$\hat{H}_B = \sum_k \hbar\omega_k \hat{b}_k^\dagger \hat{b}_k, \quad (3)$$

$$\hat{H}_C = \hat{\sigma}_x \sum_k \frac{v_k}{2} (\hat{b}_k^\dagger + \hat{b}_k). \quad (4)$$

The model system consists of a single spin which has an energy-level splitting $\hbar\Delta$. The model bath consists of bosonic modes k with natural frequencies ω_k . The boson creation and annihilation operators satisfy $[\hat{b}_k, \hat{b}_l^\dagger] = \delta_{kl}$. The coupling between the system and bath is here chosen to be transverse [24] and occurs via the bath operator

$$\hat{X} = \sum_k v_k (\hat{b}_k^\dagger + \hat{b}_k). \quad (5)$$

The couplings v_k are real numbers (possible phases were absorbed into the definitions of the boson operators). A generalization to the multi-spin case is straightforward and is presented in Appendix A.

The effect of the bath on the system is fully determined by a bath spectral function. The spectral function is defined as:

$$S(\omega) = \int_{-\infty}^{\infty} dt e^{i\omega t} \left\langle \hat{X}(t) \hat{X}(0) \right\rangle_0, \quad (6)$$

where the index 0 refers to an average according to a free evolution of the bath. This function plays a central role in the bath mapping presented later. In thermal equilibrium we have:

$$S(\omega) = 2\pi \sum_k \frac{v_k^2 \delta(|\omega| - \omega_k)}{1 - \exp\left(-\frac{\hbar\omega}{k_B T}\right)} \text{sign}(\omega). \quad (7)$$

The spectral function is characterized by two essential properties: the temperature T , as well as its overall functional form. The temperature controls the symmetry between the positive (photon absorption by the bath) and negative (photon emission by the bath) frequencies. The functional form of the spectral function is important in the sense that it is not a constant and therefore does not correspond to white noise. In particular, this implies that the bath has a memory, *i.e.*, it is non-Markovian.

The wide applicability of the spin-boson theory is based on the fact that the bath described by \hat{H}_B does not necessarily need to consist microscopically of bosonic modes, but need only be effectively Gaussian. An example of such bath is given in Appendix E, where we derive a spin-boson model of a spin coupled to an electronic bath.

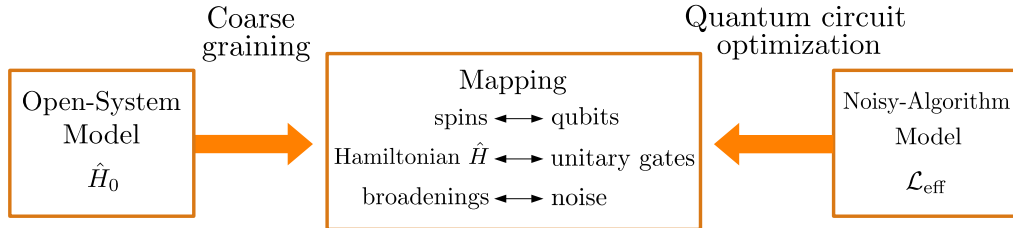


FIG. 1: Bath mapping, *i.e.*, mapping between an open-system model and a noisy-algorithm model. As described in the main text, the open-system model \hat{H}_0 is first coarse grained to an auxiliary-spin model \hat{H} and additional spin broadenings. A quantum algorithm time evolves the qubits describing the spins according to \hat{H} . The combined effect of unitary gates and non-unitary qubit noise is described by an effective Lindbladian \mathcal{L}_{eff} . The auxiliary-spin model broadening and the noise broadening according to \mathcal{L}_{eff} are set equal by choosing the Trotter time step correctly. A circuit optimization may be needed to have \mathcal{L}_{eff} in a desired form.

III. BATH MAPPING

At the center of our approach is a mapping between an open-system model and a noisy-algorithm model. The mapping is visualized in Fig. 1. The open-system model is first represented using a model that includes only spins, with Hamiltonian \hat{H} , and additional spin broadenings. The spins are represented by qubits on a quantum computer. The noisy-algorithm model, on the other hand, describes the Trotterized time evolution according to \hat{H} as a static Lindbladian \mathcal{L}_{eff} operating on a time-evolved density matrix [22]. The spin broadenings and the noise described by \mathcal{L}_{eff} are made equivalent by choosing the Trotter time step τ correctly. The full self-consistent procedure is described in more detail below.

A. Coarse graining

In this part of the mapping, we reduce the number of bath modes in the open-system model from infinite to n modes with broadening. These broad modes are now called auxiliary boson modes. As a practical matter, in this step we fit the target spectral function by n Lorentzians. We also write down a Lindblad master equation that is equivalent to this coarse-grained spectral function.

1. Coarse graining when only the bath qubits are noisy

In this common coarse-graining scheme, the target spectral function, Eq. (7), is fitted by n Lorentzians,

$$S(\omega) = \sum_{i=1}^n v_i^2 \frac{\kappa_i}{(\kappa_i/2)^2 + (\omega - \omega_i)^2}. \quad (8)$$

Here we use the counting index i instead of k , referring to the auxiliary modes. The fitting is done by optimizing the peak areas $2\pi v_i^2$, frequencies ω_i , and broadenings κ_i . Later, the broadenings will be mapped to qubit noise. Therefore, in the fitting, the relative sizes of the

broadenings need to be fixed so that they will be consistent with the effective noise given by the noisy-algorithm model \mathcal{L}_{eff} (Sec. III C). The absolute size (a common prefactor) is a free fitting parameter, since it will correspond to choosing the Trotter time step τ .

The couplings and frequencies obtained in the fitting correspond to parameters of the Hamiltonian

$$\hat{H} = \hat{H}_S + \hat{\sigma}_x \sum_{i=1}^n \frac{v_i}{2} (\hat{b}_i^\dagger + \hat{b}_i) + \sum_{i=1}^n \hbar \omega_i \hat{b}_i^\dagger \hat{b}_i, \quad (9)$$

and the mode broadenings to damping rates in the Lindblad master equation:

$$\dot{\hat{\rho}} = \frac{i}{\hbar} [\hat{\rho}, \hat{H}] + \sum_{i=1}^n \kappa_i \left(\hat{b}_i \hat{\rho} \hat{b}_i^\dagger - \frac{1}{2} \{ \hat{b}_i^\dagger \hat{b}_i, \hat{\rho} \} \right), \quad (10)$$

where $\hat{\rho}$ is the density matrix of the spin and the auxiliary boson modes.

It should be noted that similar coarse graining approaches have also been applied earlier, for example, in the context of Lindbladian description of non-Markovian baths [25–30] and analog quantum simulation [24, 31–33]. This approach is also closely related to the approach of hierarchical equations of motion [34–36].

2. Coarse graining when the system qubit is also noisy

The fitting process can also account for decoherence of a qubit representing the (system) spin. The decoherence of this system qubit contributes via a background rate in the spectral function. Here, we instead optimize the spectral function

$$S(\omega) = \sum_{i=1}^n v_i^2 \frac{\kappa_i}{(\kappa_i/2)^2 + (\omega - \omega_i)^2} + 4\hbar^2 \kappa_{\text{system}}, \quad (11)$$

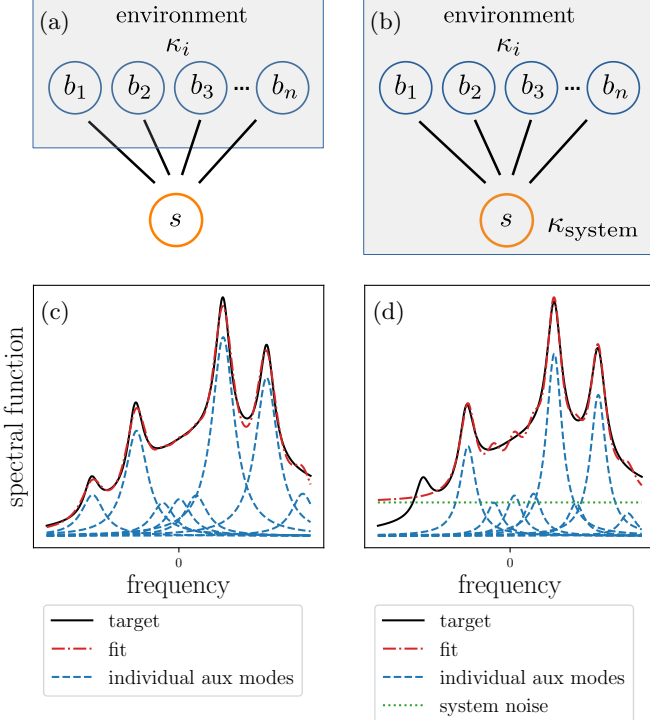


FIG. 2: Fitting of a target spectral function in the two discussed bath-mapping schemes. (a) The system spin s couples to n auxiliary boson modes b_1, \dots, b_n . The auxiliary modes further couple to an environment, which leads to mode broadenings κ_i . (b) In the second scheme, also the system spin couples to the environment, which leads to a decoherence rate κ_{system} . (c) An example of fitting by eight auxiliary modes without system noise. All modes are assumed to have the same broadening. (d) An example of fitting the same spectral function but in the presence of system noise. The system noise contributes via a constant shift of the fitting function, leading to a different set of optimal auxiliary-mode parameters.

where the ratio between the system noise and the average bath broadening is fixed to certain constant ratio r ,

$$\kappa_{\text{system}} = r \langle \kappa_i \rangle. \quad (12)$$

This ratio is defined not only by the quantum hardware properties, but also by the algorithm which is used. If the system and bath qubits have equal decoherence rates, we can have $r = 1$ or $r = 1/2$ (the latter if a noise-symmetrization algorithm is applied, as in Sec. IV C).

The spectral function of Eq. (11) corresponds to a time evolution according to the Lindblad master equation

$$\begin{aligned} \dot{\hat{\rho}} = \frac{i}{\hbar} [\hat{\rho}, \hat{H}] + \sum_{i=1}^n \kappa_i \left(\hat{b}_i \hat{\rho} \hat{b}_i^\dagger - \frac{1}{2} \{ \hat{b}_i^\dagger \hat{b}_i, \hat{\rho} \} \right) \\ + \kappa_{\text{system}} (\hat{\sigma}_x \hat{\rho} \hat{\sigma}_x - \hat{\rho}). \end{aligned} \quad (13)$$

The difference to Eq. (10) is the term proportional to

κ_{system} . We see that the system (collapse) operator in this term is $\hat{\sigma}_x$. It follows that the bath mapping in this scheme is exact if the system-qubit noise operator (in the corresponding noisy-algorithm model) is also proportional to $\hat{\sigma}_x$. An exact mapping can be obtained also in the case of all qubits being subject to damping, after a noise-symmetrization algorithm, as shown in Sec. IV C. More generally, the bath mapping in such a scheme is most likely only an approximation (when, for example, the system is subjected to depolarising noise) but can work well for a weak coupling between the system and the bath. The fitting in the two different schemes is illustrated in Fig. 2.

B. Representing auxiliary bosons by auxiliary spins

Here we write down a Lindblad master equation that includes only spins and is equivalent with the coarse-grained spin-boson model. For this, we represent the derived auxiliary boson modes by auxiliary spins. Common digital encodings [37] cannot be applied, since they do not map damping of an arbitrary auxiliary spin to single-boson annihilation, which is the key correspondence in our algorithm. Instead, we replace bosonic energy operators $\hat{b}^\dagger \hat{b}$ by a sum of auxiliary spin operators $\hat{\sigma}_z^j/2$ and bosonic coupling operators $\hat{b}^\dagger + \hat{b}$ by a sum of auxiliary spin operators $\hat{\sigma}_x^j$. The spectral function, Eq. (8) or (11), keeps its form, with the summation performed now over the corresponding auxiliary-spin parameters. There is no strict rule how the auxiliary-boson and auxiliary-spin parameters should be exactly related. Two possible approaches are discussed below.

A straightforward approach is to replace each derived auxiliary boson mode i by N_i identical auxiliary spins. This allows one to keep the spectral function unchanged, by down-scaling the coupling by a factor $1/\sqrt{N_i}$, with a control of the bath Gaussianity through varying N_i , *i.e.*, by being able to keep the excitation numbers of individual auxiliary spins low by increasing N_i . This approach can be applied if the bath qubits have similar decoherence rates, since the auxiliary spins are mapped later to bath qubits. The coarse-grained model Hamiltonian, represented now by only spins, becomes

$$\hat{H} = \hat{H}_{\text{S}} + \hat{\sigma}_x \sum_{i=1}^n \frac{v_i}{2} \sum_{j=1}^{N_i} \frac{1}{\sqrt{N_i}} \hat{\sigma}_x^{i,j} + \sum_{i=1}^n \frac{\hbar \omega_i}{2} \sum_{j=1}^{N_i} \hat{\sigma}_z^{i,j}. \quad (14)$$

However, if significant differences exist in the bath-qubit decoherence rates, it may be better if one imposes one-to-one correspondence between the auxiliary-boson modes and the auxiliary spins, *i.e.*, fixes $N_i = 1$. These two approaches are visualized in Fig. 3.

It is very valuable for the bath mapping that for auxiliary spins the spectral-peak broadening can be theoretically not only due to the damping rate γ but also due

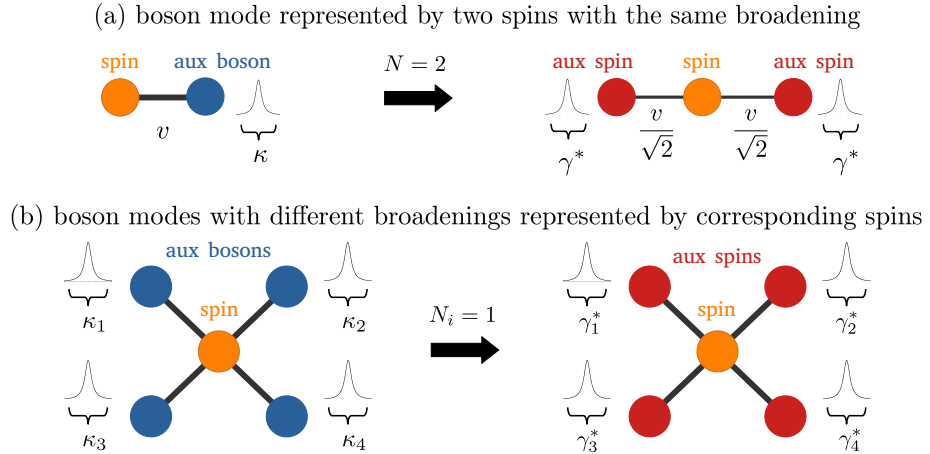


FIG. 3: Principles of two possible approaches for representing auxiliary bosons by auxiliary spins (and finally by bath qubits). (a) The coarse-grained spin-boson model includes one spin coupled to one auxiliary boson mode. The auxiliary boson mode is chosen to be represented by $N = 2$ identical auxiliary spins. The new couplings are down-scaled by a factor $1/\sqrt{N}$ in order to keep the total spectral weight unchanged. We have $\kappa = \gamma^*$, where the effective spin broadening is a sum of spin damping and dephasing, $\gamma^* = \gamma + 2\Gamma$. This mapping approach can be applied if the bath qubits representing the auxiliary spins have relatively homogeneous broadenings. (b) An approach that can be applied when the bath qubits have significantly differing broadenings. Here one imposes one-to-one correspondence between the boson modes and the auxiliary spins.

to the dephasing rate Γ ,

$$\kappa_i = \gamma_i + 2\Gamma_i \equiv \gamma_i^*. \quad (15)$$

This property is important since it allows one to do the mapping also when the bath qubits are subjected to significant dephasing. The corresponding Lindbladian has the form (for simplicity considering here $N_i = 1$)

$$\begin{aligned} \dot{\hat{\rho}} = \frac{i}{\hbar} [\hat{\rho}, \hat{H}] + \sum_{i=1}^n \gamma_i \left(\hat{\sigma}_+^i \hat{\rho} \hat{\sigma}_-^i - \frac{1}{2} \{ \hat{\sigma}_+^i \hat{\sigma}_-^i, \hat{\rho} \} \right) \\ + \sum_{i=1}^n \frac{\Gamma_i}{2} (\hat{\sigma}_z^i \hat{\rho} \hat{\sigma}_z^i - \rho). \end{aligned} \quad (16)$$

It should be noted that broadening due to dephasing alone does not lead to Gaussian equilibrium statistics: a finite damping rate γ is needed. This is because certain bath correlations that describe non-bosonic statistics decay in time according to γ instead of $\gamma + 2\Gamma$.

C. Matching spin broadening with qubit noise

Here we describe how the Lindblad master equation operating only on spins can be implemented in digital quantum computing by using noise. The key part is the matching of the spin broadening with the effective qubit noise. This step should be done self-consistently with the coarse graining (Sec. III A): variations in the effective noise of qubits must appear as corresponding relative variations in the auxiliary-mode broadenings κ_i .

We need to assume that the intrinsic and the effective noise is predominantly qubit/spin damping and dephas-

ing. The form of the effective noise can however depend on the choice of gate decompositions, which needs to be taken into account when designing the quantum circuits. This is detailed in Appendices B and C.

In the considered case, the noisy-algorithm model [22] gives the effective spin damping and dephasing rates:

$$\gamma_i = \frac{Dt_{\text{gate}}\bar{\gamma}_i}{\tau}, \quad (17)$$

$$\Gamma_i = \frac{Dt_{\text{gate}}\bar{\Gamma}_i}{\tau}, \quad (18)$$

where D is the depth of one Trotter-step circuit, t_{gate} is the physical time needed to perform one gate (assumed here to be a constant), $\bar{\gamma}_i$ and $\bar{\Gamma}_i$ are the physical damping and dephasing rates of the qubit representing the auxiliary spin i , and τ is the chosen Trotter time step. We assume here that the errors are similar for every gate and that they act also on qubits that are at rest. The potential variation in the widths $\gamma_i + 2\Gamma_i$ needs to be accounted for in the coarse graining, as discussed above. The contribution from finite system qubit noise is similar.

Eqs. (17-18) with Eq. (15) can be used to solve the Trotter time step τ , which was still a free parameter. This solution corresponds to matching the spin broadening with the effective qubit noise. For simplicity, let us now assume that all bath qubits have homogeneous damping and dephasing rates. We obtain

$$\tau = \frac{D\epsilon}{\kappa}, \quad (19)$$

where we have defined the gate error parameter

$$\epsilon \equiv t_{\text{gate}}(\bar{\gamma} + 2\bar{\Gamma}). \quad (20)$$

In terms of qubit decay time $T_1 = 1/\bar{\gamma}$ and pure dephasing time $T_\Phi = 1/\bar{\Gamma}$, this is defined equivalently

$$\epsilon = t_{\text{gate}} \left(\frac{1}{T_1} + \frac{2}{T_\Phi} \right). \quad (21)$$

In comparison to other error metrics in the literature [38, 39], the contribution from pure dephasing is here doubled. This is because we do not average over the Bloch sphere, but instead look at noise in the Z-basis. When all qubits are subject to damping only, the corresponding one-qubit Pauli (or average) error is $\epsilon/2$ ($\epsilon/3$) and the two-qubit error is ϵ ($4\epsilon/5$).

Since all terms of the normalized Hamiltonian \hat{H}/κ are fixed in the coarse graining, Eq. (19) gives the angles of the unitary gates $\exp(-i\hat{H}\tau)^m = \exp(-iD\epsilon\hat{H}/\kappa)^m$, *i.e.*, the angles of the unitary gates in the Trotterization of the time-evolution operator over simulation time $t = m\tau$. The mapping procedure is now completed.

IV. EXAMPLES

In this section we present examples of solving open-system dynamics using our quantum algorithm. We solve dynamics for three different open system models and study the quality by comparing to exact or approximate solutions derived in the literature. In Sec. IV A, we study the dynamics of a spin coupled ultra-strongly to a resonance mode with broadening. In Sec. IV B, we study a spin coupled to an ohmic bath. In these examples we assume that the quantum computer has a noiseless system qubit. In Sec. IV C, we study the steady state and relaxation dynamics of strongly interacting electrons hopping between an island and leads. In this example, the system qubit is allowed to be noisy too. The numerical results shown for the Trotterized time evolution were obtained using qoqo [40] with QuEST [41] as the simulator backend, by solving the time evolution of the density-matrix of the qubits.

A. Spin coupled ultra-strongly to a resonance mode with broadening

Here we study the case of a bath with a resonance frequency. We assume a Lorentzian spectral function, which can be coarse grained exactly by single auxiliary boson mode (sec. III A). The coarse-grained open-system model has the Hamiltonian:

$$\hat{H} = \frac{\hbar\Delta}{2}\hat{\sigma}_z + \frac{v}{2}\hat{\sigma}_x(\hat{b}^\dagger + \hat{b}) + \hbar\omega_0\hat{b}^\dagger\hat{b}. \quad (22)$$

We consider the case of ultra-strong coupling, $v = \omega_0 \sim \Delta$, and $\kappa = v/2$, which leads to clear non-Markovian system-bath dynamics.

In the next step of the bath mapping, the auxiliary boson mode is represented by N auxiliary spins (Sec. III B). On the quantum computer, auxiliary spins correspond to bath qubits. We assume all bath qubits have the same damping and dephasing rates, $\bar{\gamma}$ and $\bar{\Gamma}$. We assume a significant dephasing by setting $\bar{\Gamma} = \bar{\gamma}/2$ ($T_\Phi = 2T_1$). The time evolution is performed according to a Trotter expansion of the time-evolution operator $\exp(-i\hat{H}\tau)^m$, decomposed into different two-qubit gates (see below), with total simulated time $t = m\tau$. The Trotter time step τ is chosen so that the auxiliary-spin broadening κ matches to the effective qubit noise, see sec. III C.

In Fig. 4, we show the time evolution of the expectation value $\langle \hat{\sigma}_x(t) \rangle$ after the system spin is excited to $+1$ eigenstate of $\hat{\sigma}_x$. The bath mode is initially at ground. In Fig. 4(a), we compare the solutions obtained when using different number of bath qubits N (auxiliary spins) to the numerically exact solution of the bosonic open-system model. The time evolution on the quantum computer is implemented using variable MS two-qubit gates, which is a native gate of the time-evolved Hamiltonian, Eq. (14). We see that the quantum-algorithm solution approaches the correct one when the bath-qubit number N is increased. This demonstrates that the algorithm works for bath qubits subjected to damping and dephasing, and that the auxiliary-spin bath behaves like one bosonic mode after multiple spins are used to represent it. The latter result is due to the ultra-strong coupling between the system and bath. For weak system-bath couplings, $N = 1$ would be adequate. The gate errors used [Eqs. (20-21)] are 1%, 3%, 5% for $N = 8, 2, 1$, correspondingly. They are chosen to be large but having negligible Trotter error (Trotter error increases with gate error).

In Fig. 4(b), we study the use of a non-native gate decomposition. We show the result for a CNOT-decomposition with restricting to the case of $N = 8$ bath qubits. The optimal decomposition consists here of a CNOT, a small-angle X-rotation, and another CNOT. There are still two versions of this circuit: either the system qubit being the control qubit (CNOT-S) or the bath qubits being the control qubits (CNOT-B). The results differ since the CNOT operation as well as the noise properties are not symmetric with interchanging the system and bath. In the plotted case of CNOT-S, we find a noticeable difference to the correct open-system model result, which implies significant changes in \mathcal{L}_{eff} . It can be derived analytically (Appendix B), that here its approximate form includes system-qubit dephasing. This emerges even though the physical system-qubit is noiseless. In Fig. 4(b), we also compare to an open-system model, where such a bath component is included as an additional coupling term $H'_C = \hat{\sigma}_z \sum_i v'_i(\hat{a}_i + \hat{a}_i^\dagger)/2$, where operators \hat{a} describe an additional bosonic bath. We

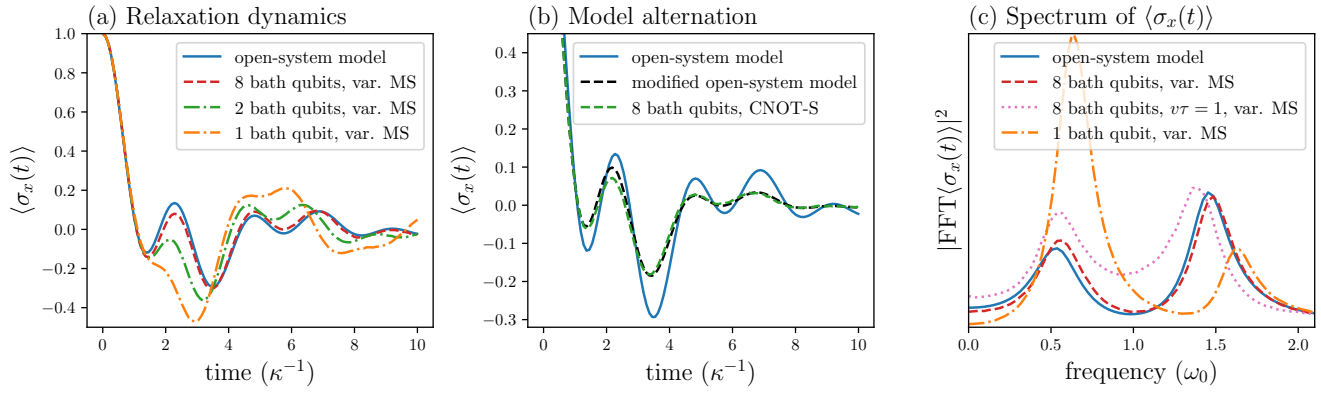


FIG. 4: Open-system dynamics of a spin coupled to a broad bosonic mode solved using the quantum algorithm and a comparison to the numerically exact solution (open-system model). We plot the time evolution of $\langle \hat{\sigma}_x(t) \rangle$ when the system spin is initially excited to $+1$ eigenstate of $\hat{\sigma}_x$ and the bath mode is at ground. When time evolving on the quantum computer, the bath qubits are subject to damping and dephasing. We consider model parameters $v = \omega_0 = 2\kappa$ and in (a-b) $\Delta = 0.9\omega_0$, in (c) $\Delta = \omega_0$. (a) An agreement with the open-system model is achieved when multiple qubits are used to represent the significantly populated bosonic mode. This improves the Gaussianity of the quantum-algorithm bath. We consider here a native (variable MS) gate decomposition and a gate error of 1%, 3%, and 5% for $N = 8, 2, 1$, respectively. (b) When $N = 8$, the result for the non-native decomposition CNOT-S (system as control) matches to a modified open-system model, where a system-spin dephasing has been added. We consider here a gate error of 0.36%. (c) The spectrum of $\langle \hat{\sigma}_x(t) \rangle$ is characterized by a peak splitting by coupling v . Also plotted is the result for a large Trotter step $v\tau = 1.0$, corresponding to a gate error of 5.6%.

find that the differences in the quantum-algorithm results indeed map well to such alternation in the original spin-boson problem. We have then recovered the open-system model the quantum computer is effectively simulating [22]. In the case of CNOT-B decomposition, we find only a small difference to the native decomposition result (not plotted). This is since here the bath qubits are never operated by X-gates. This result underlines the observation that large-angle rotations of bath qubits should be avoided. The results for optimal control-Z decompositions are similar to CNOT-B (Appendix C).

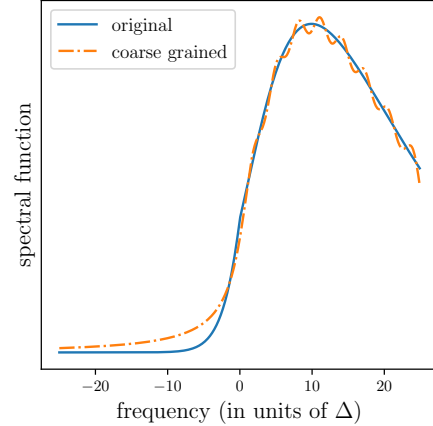


FIG. 5: Fitting of an ohmic spectral function with exponential cutoff by eight broad (auxiliary) boson-modes. The fitting is done with a constriction of auxiliary modes having identical broadenings $\kappa_i = \kappa$.

In Fig. 4(c), we study the spectrum of the obtained time evolutions. We plot here the absolute square of the Fast Fourier Transform (FFT) of $\langle \hat{\sigma}_x(t) \rangle$. The correct open-system model result shows a splitting of a resonance located originally at ω_0 to frequencies $\omega_0 \pm v/2$. This is reproduced well by the quantum algorithm with the bath-qubit number $N = 8$ and the gate error of 1% (Trotter step $v\tau = 0.18$). We also show the result for a very large Trotter step, $v\tau = 1.0$ and $N = 8$, corresponding to a gate error as large as $\epsilon = 5.6\%$. We find that this result, with non-negligible Trotter error, is clearly closer to the correct result than the one with $N = 1$ and the gate error of 5% ($v\tau = 0.2$), which has significant Gaussianity error. This result is specific for the case of ultra-strong coupling, where the bath excitation number is large and needs to be accounted for by large N , with the possible cost of increased Trotter error. An error tradeoff in the quantum algorithm is discussed more in Appendix D.

B. Spin coupled to an ohmic bath

The case of an ohmic bath emerges in many areas of physics and highlights how the system-bath dynamics can drastically change with the system-bath interaction strength. We now show that this behavior is reproduced correctly by the presented quantum algorithm.

An ohmic spectral function has the form,

$$S(\omega) = \frac{4\pi\hbar^2\alpha\omega}{1 - \exp\left(-\frac{\hbar\omega}{k_B T}\right)}, \quad (23)$$

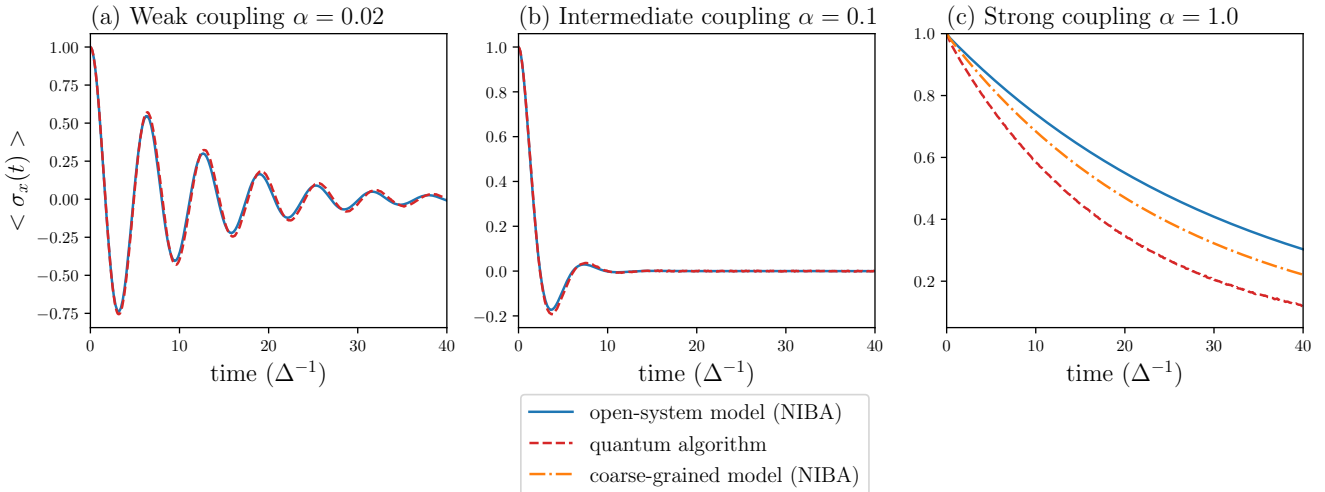


FIG. 6: Open-system dynamics of a spin coupled to an ohmic bath solved using the quantum algorithm and a comparison to the numerical solution obtained using the NIBA (Non-Interacting Blip Approximation). We use a variable MS decomposition and a gate error of 5%. In the quantum algorithm, the ohmic bath is represented by eight auxiliary boson-modes with a coarse-grained spectral function as shown Fig. 5. Each of the boson modes is represented by one bath qubit. We show the NIBA result also for the coarse-grained spectral function in the case of strong coupling $\alpha = 1$ (while for $\alpha = 0.02$ and $\alpha = 0.1$ the differences are negligible). We find that the famous transition from a weak damping to a slow decay with increasing α is reproduced well by the quantum algorithm.

where the interaction strength is characterized by the so-called Kondo parameter α as well as the temperature T . We choose $k_B T / \hbar \Delta = 1.5$, where $\hbar \Delta$ is the spin splitting. We also introduce a cutoff function $\exp(-|\omega|/\omega_c)$ with $\omega_c/\Delta = 10$. The coarse graining is done by eight auxiliary boson-modes with a constriction to identical broadenings $\kappa_i = \kappa$ and is shown in Fig. 5.

In the quantum algorithm, we choose to represent each of the auxiliary boson modes by one auxiliary spin. When time evolving on the quantum computer, we assume that the corresponding bath qubits are subjected only to damping. The quantum algorithm is of the same form as for the resonant bath considered in Sec. IV A, with the difference that here the auxiliary spin parameters are not identical. We consider the case of variable MS decomposition and a gate error $\epsilon = 5\%$ ($\Delta\tau = 0.11$). The conclusions made for the use of different gate decompositions in Sec. IV A are valid here as well.

In Fig. 6, we show the time evolution of $\langle \hat{\sigma}_x(t) \rangle$ when the system-spin is again set initially to the $+1$ eigenstate of $\hat{\sigma}_x$ and when the bath is initially at equilibrium. We show the resulting dissipative dynamics for weak, intermediate, and strong coupling limits, corresponding to $\alpha = 0.02, 0.1, 1.0$. We compare the quantum algorithm results to the so-called NIBA (non-interacting blip approximation) calculation of the same dynamics [6, 42]. We perform this calculation for the original ohmic spectral function as well as for the coarse-grained spectral function. Since a noticeable difference appeared only for strong couplings, the latter result is shown only for $\alpha = 1.0$. We find that the celebrated transition, from a weak-to-strong damping and finally to a slow decay, is reproduced well by the quantum algorithm. We find

a good agreement with the NIBA even though each of the auxiliary boson modes is represented by only one auxiliary spin. A difference to the NIBA emerges only for large α . This difference is due to a combination of imperfect fitting (see the result for the NIBA with the coarse-grained bath) and elevated bath-qubit populations at low-frequencies.

C. Electronic transport models

In the third example, we time evolve open-system dynamics according to a generalized spin-boson model that can describe electronic transport, for example, across metallic islands or quantum dots. This model is also interesting since it may allow for mapping system-qubit damping to the coarse-grained spectral function exactly. The Hamiltonian $\hat{H}_0 = \hat{H}_S + \hat{H}_B + \hat{H}_C$ has the form

$$\begin{aligned} \hat{H}_S &= \frac{\hbar\Delta}{2} \hat{\sigma}_z, \\ \hat{H}_B &= \sum_k \hbar\omega_k \hat{a}_k^\dagger \hat{a}_k + \sum_k \hbar\omega_k \hat{b}_k^\dagger \hat{b}_k, \end{aligned} \quad (24)$$

$$\hat{H}_C = \hat{\sigma}_x \sum_k \frac{v_k}{2} (\hat{a}_k^\dagger + \hat{a}_k) + \hat{\sigma}_y \sum_k \frac{v_k}{2} (\hat{b}_k^\dagger + \hat{b}_k). \quad (25)$$

The model bath has two sets of bosonic modes, described by the bosonic operators \hat{a} and \hat{b} , coupled to the system via operators $\hat{\sigma}_x$ and $\hat{\sigma}_y$. The spectral functions of these individual baths are defined similarly as before, Eq. (7), and are here identical. An example of an open quantum system that can be modeled with this Hamiltonian is a system of two coupled islands, where the system is the two-level system and the bath is the environment between the islands.

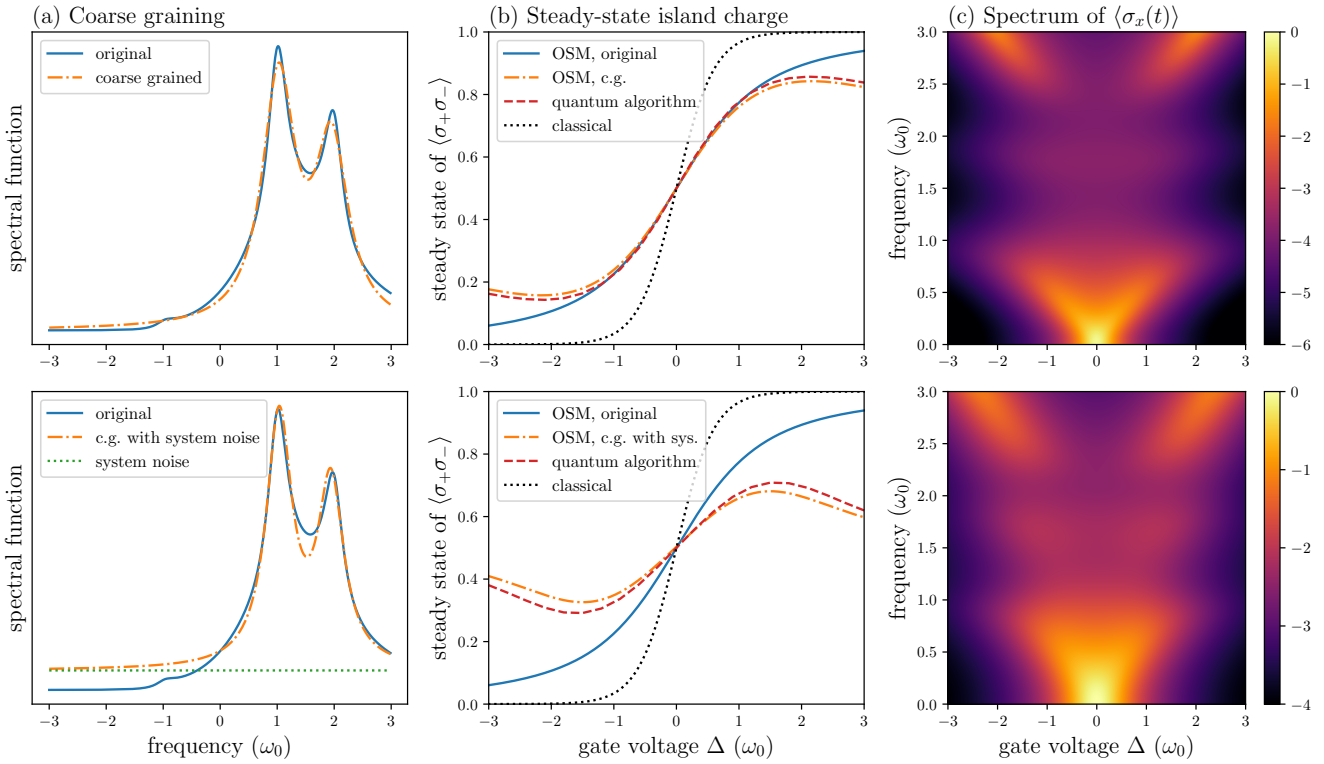


FIG. 7: The steady-state and relaxation dynamics of a single-electron transistor island-charge, solved using two quantum algorithms (above, without system noise, below, with system noise), and a comparison to a numerical solution obtained by a method presented in Ref. [43] (referred as the open-system model, OSM). We set the source-drain bias to zero and vary the gate voltage Δ . Both algorithms are based on variable MS gate decomposition and a gate error of 1%. (a) Fitting of the resonant spectral function by two modes with identical broadenings (above) and by two modes with identical broadenings and system noise (below). (b) A comparison between the solutions for the steady-state island charge. We calculate the OSM solution for the original spectral function as well as for the coarse-grained spectral function. A difference appears at high gate voltages due to an increased effective temperature of the coarse-grained bath at high energies. In the presence of the system-qubit noise (below), a difference to the original open-system model result appears at all gate voltages due to an increased effective temperature at all energies. The quantum algorithm result and the OSM result for the coarse-grained bath however stay similar. (c) The spectrum of the charge relaxation dynamics (log-scale) when initially setting the island charge to +1 eigenstate of $\hat{\sigma}_x$. A peak tripling appears in the vicinity of the bath resonances. When solved with the algorithm with system noise (below), additional broadening appears but the key characteristics remain.

nian is a single-electron transistor (Appendix E). Here, for strongly interacting electrons only two island-charge states are relevant, and these are mapped to the two states of the introduced system-spin. The gate voltage of the transistor translates into the energy-level splitting Δ . The source-drain bias is assumed to be here zero.

We construct two quantum algorithms for solving this problem. The first one is designed for a quantum hardware with a noiseless system-qubit and bath qubits that are subjected to damping noise, and the second algorithm for all qubits being noisy. Furthermore, we consider a structured spectral function $S(\omega)$, which is ohmic at low frequencies, has resonances at ω_0 and $2\omega_0$, and is at relatively low temperature $k_B T = 0.3\hbar\omega_0$ (Appendix E). This can describe transmission lines with resonances. The system-bath coupling is of similar magnitude as the resonance mode broadening. The spectral function fitting corresponding to the two algorithms is shown in Figs. 7(a).

In the algorithms, each auxiliary boson mode is represented by one bath qubit. We have in total four bath qubits (two independent baths). On hardware, this could be realized by a system qubit with four neighboring bath qubits. We use a variable MS decomposition and a gate error of 1%. In the case of noisy system qubit, X-gates are introduced between the original Trotter-step circuits in order to transform damping to a sum of X-noise and Y-noise, which allows it to be mapped to the spectral function, see Appendix C. We have a background rate factor $r = 1/2$, see Sec. III A 2.

In Fig. 7(b), we show the obtained steady-state values for the island charge $\langle \hat{\sigma}_+ \hat{\sigma}_- \rangle$ as a function of the gate voltage Δ . We also do a comparison to an open-system model solution obtained by applying the numerical method developed in Ref. [43]. We again apply the reference method to the original spectral function as well as to the coarse-grained spectral function. The shown classical solution is the result in the limit $\alpha \rightarrow 0$ and cor-

responds to the Fermi function. In the case of a noiseless system qubit (above plot), we find a good agreement between the quantum algorithm result and the open-system model solution. In particular, all different results (except the classical one) are practically identical when the bias Δ/\hbar is at the well-fitted spectral-function region. For larger $|\Delta/\hbar|$, differences appear due to imperfect coarse graining. However, importantly, the results for the same spectral functions stay practically identical. The coarse-grained spectral function can be interpreted as describing a non-equilibrium bath, with elevated temperature at higher energies. When all qubits are subject to damping (bottom plot), the steady-state island charge is now different for all gate voltages, when comparing to the original open-system model solution. However, the results for the same spectral functions stay again almost identical. This confirms that the system-qubit noise can indeed be mapped to the spectral function of the open-system model.

In Fig. 7(c), we study the dynamical behavior of the island charge, when exciting the island charge initially to symmetric superposition, *i.e.*, to $+1$ eigenstate of σ_x . We present the result for the spectrum of $\langle \hat{\sigma}_x(t) \rangle$. In the case of the noiseless system qubit (above plot), we find that far from the resonances $\Delta = \omega_0$ or $\Delta = 2\omega_0$, a narrow peak appears at frequency $\omega \approx \Delta$. This corresponds to coherent phase oscillations between the charge states with exponential decay of the coherence. The system-bath dynamics are Markovian. Closer to the bath resonances, the peak shows strong broadening as well as splitting into a triplet. We find that in this region the underlying system-bath dynamics is non-Markovian, which occurs due to the strong system-bath coupling. We also see that the same key characteristics appear when solving the problem with the algorithm with system noise (bottom plot). This highlights that dynamics of open quantum systems with a structured bath can be solved with the presented quantum algorithm also in the presence of strong system-qubit noise.

V. DISCUSSION

In this work we have developed a new framework for noise-utilizing quantum simulations. The presented quantum algorithms map typical noise in digital quantum computing to spectral function properties of open system models. At the center of this approach is the noisy-algorithm model, which describes the effect of noise in the form of a static Lindblad master equation operating on the time-evolved density matrix [22].

The form of this static Lindbladian depends on the used circuit decomposition. In the examples we have considered, optimal circuit decompositions were based on native gates, such as the small-angle single-qubit rotations, variable MS two-qubit gates (XX interaction), or variable iSWAP two-qubit gates (XX + YY interaction). We also found that non-native gate decompositions can

work as well, but may lead to alternations to the actually time-evolved open-system model. The examples considered also showed that the algorithm can perform very well even with gate errors as high as 1%. The performance however improves with decreasing gate error. It is thus beneficial to have as low of a gate error as possible. The central parameters used in the examples are summarized in Table I.

In the shown examples we considered single-spin systems. It should be emphasized that the quantum algorithm can be applied also to multi-spin systems, such as exciton-transport models [5]. Actually, the algorithm is most efficient when time evolving a model with multiple system spins, due possibility to more efficient gate parallelization. More specifically, for a fixed number of bath modes, system spins can be added without additional cost (*e.g.*, decrease in the needed gate error) when exploiting all-to-all connectivity or the system-bath SWAP algorithm presented in Appendix C.

The derivation of the quantum algorithm assumed the use of qubits with intrinsic noise that can be described using a Lindbladian formalism. However, we note that the approach is also directly applicable to more general quantum elements and noise whose effect is rather of Bloch-Redfield form. Furthermore, the general principles of modifying the effective noise could also be applied to general non-Markovian noise. Utilization of non-Markovian noise in quantum computing has been addressed recently in Ref. [44].

The focus in this article has been on utilizing intrinsic qubit noise. However, it is indeed also possible that one may implement the required non-unitary operations through the use of measurements [7, 9–12, 14–17]. The desired large difference in decoherence rates between the system and bath qubits could in fact be implemented more easily within such approach. One could consider algorithms that are based on combining both of these approaches. The bath qubits may also be replaced by resonators or phonon modes on hardware [24, 31–33] with engineered damping.

Finally, the quantum algorithm and conclusions presented in this paper are not restricted to simulating the spin-boson model, but are applicable also for more general open-system models.

Acknowledgments

This work was supported by the German Federal Ministry of Education and Research, through PhoQuant (13N16107), and QSolid (13N16155), and by the German Federal Ministry of Economic Affairs and Climate Action, through the PlanQK project (01MK20005H). This work was also supported by the European Union’s Horizon 2020 program number 899561, AVaQus.

Decomposition	Example A		Example B		Example C	
	Depth D	gate error ϵ (%)	Depth D	gate error ϵ (%)	Depth D	gate error ϵ (%)
Variable MS	$1 + n_q$	1	$1 + n_q$	5	$1 + 2n_q$	1
Variable iSWAP	$1 + 4n_q$	0.27	$1 + 4n_q$	1.4	$1 + 2n_q$	1
CNOT	$1 + 3n_q$	0.36	$1 + 3n_q$	1.8	$1 + 4n_q$	0.53
Control-Z	$1 + 5n_q$	0.2	$1 + 5n_q$	1.1	$1 + 6n_q$	0.36

TABLE I: Circuit depths and gate errors in the three examples presented in Sec. IV when realized using different two-qubit gate decompositions. The gate error is defined in Eqs. (20-21). Access to lower gate error ϵ allows the use of a smaller Trotter step (reduce the Trotter error) and/or a larger total number of bath qubits n_q (reduce the coarse graining and/or the bath Gaussianity error). In the three examples we have $n_q = 8, 8, 4$ respectively. We assume a system-to-all-bath device connectivity. For a nearest-neighbor connectivity, a system-bath SWAP algorithm can be applied (Appendix C), which in the case of even n_q adds to the circuit depth by $(n_q/2 - 1)n_{\text{SWAP}}$, where n_{SWAP} is the number of gates needed to perform the SWAP operation.

Appendix A: Generalization to multi-spin systems

For simplicity, the main text considers only the case of one system spin. The presented algorithm can however be generalized to cover also multi-spin systems. An example of a multi-spin Hamiltonian is

$$\hat{H}_S = \sum_{i \in \text{system}} \frac{\hbar \Delta_{ii}}{2} \hat{\sigma}_z^i + \frac{1}{2} \sum_{i < j \in \text{system}} \hbar \left(\Delta_{ij} \hat{\sigma}_+^i \hat{\sigma}_-^j + \Delta_{ij}^* \hat{\sigma}_+^j \hat{\sigma}_-^i \right), \quad (\text{A1})$$

$$\hat{H}_B = \sum_k \hbar \omega_k \hat{b}_k^\dagger \hat{b}_k, \quad (\text{A2})$$

$$\hat{H}_C = \frac{1}{2} \sum_{i \in \text{system}} \hat{\sigma}_z^i \sum_k \left(v_{ik}^* \hat{b}_k^\dagger + v_{ik} \hat{b}_k \right). \quad (\text{A3})$$

The couplings $\Delta_{i \neq j}$ and v may be complex numbers (as only a select number of phases can be absorbed into definitions of the boson operators). This Hamiltonian is commonly used to describe exciton transport in photosynthesis, where the system spins correspond to excitons and the bosonic modes to molecular vibrations.

The spectral function is defined analogously as for the single-spin system. The multi-dimensional spectral function is defined as

$$S_{ij}(\omega) = \int dt e^{i\omega t} \langle \hat{X}_i(t) \hat{X}_j(0) \rangle_0, \quad (\text{A4})$$

where

$$X_i = \sum_k (v_{ik} \hat{b}_k + v_{ik}^* \hat{b}_k^\dagger). \quad (\text{A5})$$

In thermal equilibrium,

$$S_{ij}(\omega) = 2\pi \frac{\sum_k v_{ik} v_{jk}^* \delta(\omega - \omega_k)}{1 - \exp\left(-\frac{\hbar\omega}{k_B T}\right)}, \quad \text{for } \omega > 0 \quad (\text{A6})$$

$$S_{ij}(\omega) = 2\pi \frac{\sum_k v_{ik}^* v_{jk} \delta(\omega + \omega_k)}{\exp\left(\frac{\hbar\omega}{k_B T}\right) - 1}, \quad \text{for } \omega < 0, \quad (\text{A7})$$

$$S_{ji}(\omega) = S_{ij}^*(\omega). \quad (\text{A8})$$

We see that cross-correlations ($i \neq j$) can appear if different spins couple to the same bath modes.

The coarse graining is done similarly as for the single-spin system. The original bosonic bath is replaced by n auxiliary boson modes. Each of these auxiliary modes has a central frequency ω_m , coupling to the i^{th} spin v_{im} , and broadening κ_m . The multi-dimensional spectral function that follows is

$$S_{ij}(\omega) = \sum_{m=1}^n v_{im} v_{jm}^* \frac{\kappa_m}{(\kappa_m/2)^2 + (\omega - \omega_m)^2}. \quad (\text{A9})$$

In the fitting, we optimize the cost function

$$C = \sum_{i \leq j} \int_{\omega_{\text{min}}}^{\omega_{\text{max}}} d\omega |S_{ij}(\omega) - S_{ij}^{\text{target}}(\omega)|^2, \quad (\text{A10})$$

by seeking optimal values for ω_m , v_{im} , and κ_m . The fitting problem includes n frequencies, nn_s couplings, and n broadenings, where n_s is the number of system spins. Furthermore, the system-qubit noise can be included similarly as in the case of the single-spin system (Sec. III A 2). Here, a constant background rate is added to diagonal components of $S_{ij}(\omega)$, assuming the system-qubit noise is uncorrelated. Possible differences in the system-qubit decoherence rates can be accounted for by generalizing the constant r in Eq. (12) to a vector r_j , where the index j refers to a system spin.

Appendix B: Noisy-algorithm model

Here we give a short description of our model of quantum computing with incoherent error. We assume that the noise inserted after each gate is qubit damping and dephasing. This can be justified for hardware with such intrinsic noise and for the application of small-angle gates. The form of the noise in the case of large-angle gates may vary. However, the principles of deriving the effective noise model and optimizing it remain the same. For a more detailed derivation and validity analysis of this noise model see Ref. [22].

1. Noise after gates (physical noise)

For the following discussion, we assume that the time-propagation algorithm is based on a Trotter expansion over time $t = m\tau$,

$$e^{-i\hat{H}t} = e^{-i\hat{H}m\tau} = \left[e^{-i\hat{H}\tau} \right]^m \approx \left[\Pi_j e^{-i\hat{H}_j\tau} \right]^m. \quad (\text{B1})$$

Here the Hamiltonian H is divided into partial Hamiltonians,

$$\hat{H} = \sum_j \hat{H}_j, \quad (\text{B2})$$

whose contributions to the time evolution are implemented using available unitary gates. For native (or natural) gates we have

$$e^{-i\hat{H}_j\tau} = \hat{U}_j, \quad (\text{B3})$$

whereas non-native decompositions have the form

$$e^{-i\hat{H}_j\tau} = \Pi_k \hat{U}_{j,k}. \quad (\text{B4})$$

In practice, the elementary gates $\hat{U}_{j,k}$ include large-angle operations, such as $R_x(\pi/2)$ or CNOT.

In our modeling, the physical noise is included as non-unitary operations after unitary gates,

$$\hat{U} \rightarrow \mathcal{N}\mathcal{U}. \quad (\text{B5})$$

On the right-hand side, the unitary gate is represented as a superoperator \mathcal{U} and the non-unitary noise as a Kraus operator \mathcal{N} . It is always possible to establish such description of an incoherent error, assuming it keeps qubits in their computational basis. In our modeling, also the identity gate is assumed to come with noise. In other words, the noise is acting also on idling qubits.

Assuming the effect of the noise per gate is weak, it is possible replace the Kraus superoperators by Lindbladians \mathcal{L}_j and physical gate times t_j such that

$$\mathcal{N}_j \approx 1 + t_j \mathcal{L}_j, \quad (\text{B6})$$

where \mathcal{L}_j is a Lindblad operator describing the physical noise.

2. Effective noise

Noise after the unitary gates can appear in a different form in the simulated system [22]. To understand how this noise mapping works, consider a simple example of decomposing some unitary to three elementary gates, $\hat{V} = \hat{U}_3 \hat{U}_2 \hat{U}_1$. Since unitary gates have also inverse gates, we can rewrite the noisy version of this circuit as

$$\begin{aligned} \hat{U}_3 \hat{U}_2 \hat{U}_1 &\rightarrow \mathcal{N}_3 \mathcal{U}_3 \mathcal{N}_2 \mathcal{U}_2 \mathcal{N}_1 \mathcal{U}_1 \\ &= \mathcal{N}_3 \mathcal{U}_3 \mathcal{N}_2 \mathcal{U}_3^{-1} \mathcal{U}_3 \mathcal{U}_2 \mathcal{N}_1 \mathcal{U}_2^{-1} \mathcal{U}_3^{-1} \mathcal{U}_3 \mathcal{U}_2 \mathcal{U}_1 \\ &\equiv \mathcal{N}_3 \mathcal{N}'_2 \mathcal{N}'_1 \mathcal{U}_3 \mathcal{U}_2 \mathcal{U}_1 \\ &\equiv \mathcal{N}\mathcal{V}, \end{aligned} \quad (\text{B7})$$

where $\mathcal{N} = \mathcal{N}_3 \mathcal{N}'_2 \mathcal{N}'_1$ and

$$\mathcal{N}'_1 = \mathcal{U}_3 \mathcal{U}_2 \mathcal{N}_1 \mathcal{U}_2^{-1} \mathcal{U}_3^{-1} \quad (\text{B8})$$

$$\mathcal{N}'_2 = \mathcal{U}_3 \mathcal{N}_2 \mathcal{U}_3^{-1}. \quad (\text{B9})$$

We see that the noise superoperator \mathcal{N}_1 got rotated by the unitary transformation $\mathcal{U}_3 \mathcal{U}_2$ and the noise superoperator \mathcal{N}_2 by \mathcal{U}_3 . Furthermore, under the assumption of small noise-probability we can approximate

$$\begin{aligned} \mathcal{N}_3 \mathcal{N}'_2 \mathcal{N}'_1 &\approx (1 + t_3 \mathcal{L}_3)(1 + t_2 \mathcal{L}'_2)(1 + t_1 \mathcal{L}'_1) \\ &\approx 1 + t_1 \mathcal{L}'_1 + t_2 \mathcal{L}'_2 + t_3 \mathcal{L}_3. \end{aligned} \quad (\text{B10})$$

Here, the operators in the individual Lindbladians \mathcal{L}_i are rotated by unitary gates $\hat{U}_{j>i}$ exactly in the same way as the noise superoperators were rotated by $\mathcal{U}_{j>i}$. The (noise part of) the effective Lindbladian then becomes

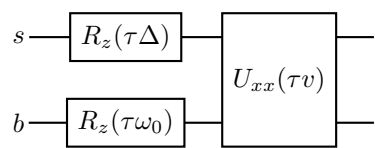
$$\tau \mathcal{L}_{\text{eff}} = t_1 \mathcal{L}'_1 + t_2 \mathcal{L}'_2 + t_3 \mathcal{L}_3. \quad (\text{B11})$$

This result can be generalized to arbitrary circuits [22].

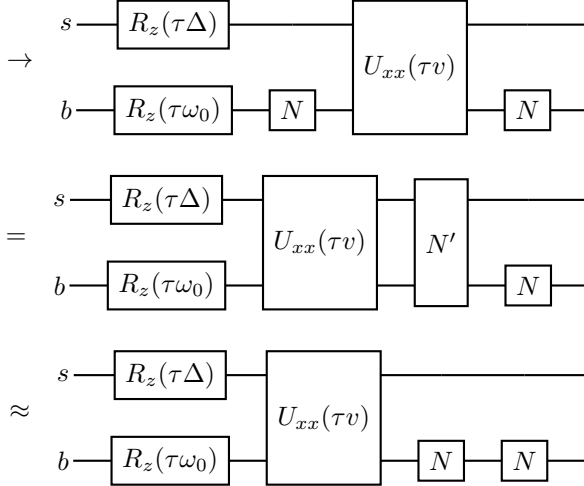
The transformation of noise to other effective forms in a series of unitary gates has also been studied recently in Refs. [15, 45, 46]. The effect of quasistatic noise in digital quantum simulation has been addressed in Ref. [47].

3. Noise transformations in the examples

In most examples we consider native XX-interaction gates. Single Trotter-step circuit of a noiseless system-qubit coupled to a noisy bath-qubit via XX-interaction is



When adding the noise model, this becomes



Here we have approximated that for the noise operator

$$\hat{N}' = \hat{U}_{xx}(\tau v) \hat{N} \hat{U}_{xx}(-\tau v) \approx \hat{N}, \quad (\text{B12})$$

which is true when $\tau v \ll 1$ and \hat{U}_{xx} is a native gate.

The derivation of the effective noise for non-native decompositions is done similarly. In the case of CNOT-B decomposition of the XX-interaction (with bath qubits as the control qubits), see Sec. IV A, we look how the control-qubit i damping and dephasing operators transform under CNOT, see Table II,

$$\text{CNOT } \hat{\sigma}_-^i \text{ CNOT} = \hat{\sigma}_-^i \hat{\sigma}_x \quad (\text{B13})$$

$$\text{CNOT } \hat{\sigma}_z^i \text{ CNOT} = \hat{\sigma}_z^i \quad (\text{B14})$$

Remember that a superscript i in a Pauli operator refers to a bath qubit (or the corresponding auxiliary spin). This tells us that physical bath-qubit damping gets translated into simultaneous bath-spin damping and system-spin flip, whereas dephasing keeps its form. This result means that the effective Lindbladian has the form

$$\begin{aligned} \mathcal{L}_{\text{eff}}[\hat{\rho}] \approx & \frac{i}{\hbar} [\hat{\rho}, \hat{H}] + (\gamma - \delta\gamma) \sum_i \mathcal{L}_{\sigma_-^i}[\hat{\rho}] + \frac{\Gamma}{2} \sum_i \mathcal{L}_{\sigma_z^i}[\rho] \\ & + \delta\gamma \sum_i \mathcal{L}_{\sigma_-^i \sigma_x}[\hat{\rho}], \end{aligned} \quad (\text{B15})$$

where we use a notation \mathcal{L}_A for a noise Lindbladian with noise operator \hat{A} . It turns out that the last term on the right-hand side of Eq. (B15) can be approximately factored into two uncorrelated contributions,

$$\begin{aligned} \mathcal{L}_{\text{eff}}[\hat{\rho}] \approx & \frac{i}{\hbar} [\hat{\rho}, \hat{H}] + (\gamma - \delta\gamma) \sum_i \mathcal{L}_{\sigma_-^i}[\hat{\rho}] + \frac{\Gamma}{2} \sum_i \mathcal{L}_{\sigma_z^i}[\hat{\rho}] \\ & + \delta\gamma \sum_i \mathcal{L}_{\sigma_-^i}[\hat{\rho}] + \gamma_{\text{system}} \mathcal{L}_{\sigma_x}[\hat{\rho}], \end{aligned} \quad (\text{B16})$$

where

$$\gamma_{\text{system}} = \delta\gamma \sum_i \langle \hat{\sigma}_+^i \hat{\sigma}_-^i \rangle. \quad (\text{B17})$$

We also get $\gamma_{\text{system}} \ll \gamma, \Gamma$, following from the fact that most of the time the individual bath qubits are at ground. It follows that γ_{system} can be neglected and we have

$$\mathcal{L}_{\text{eff}}[\hat{\rho}] \approx \frac{i}{\hbar} [\hat{\rho}, \hat{H}] + \gamma \sum_i \mathcal{L}_{\sigma_-^i}[\hat{\rho}] + \frac{\Gamma}{2} \sum_i \mathcal{L}_{\sigma_z^i}[\hat{\rho}], \quad (\text{B18})$$

This has the same form as the physical noise.

For CNOT-S, *i.e.*, when the system qubit is the control qubit, the changes in the effective model are larger. This can be derived by looking at the target-qubit noise conversions, see Table II,

$$\text{CNOT } \hat{\sigma}_-^i \text{ CNOT} = \hat{P}_0 \hat{\sigma}_-^i + \hat{P}_1 \hat{\sigma}_+^i \quad (\text{B19})$$

$$\text{CNOT } \hat{\sigma}_z^i \text{ CNOT} = \hat{\sigma}_z \hat{\sigma}_z^i, \quad (\text{B20})$$

where $\hat{P}_0 = (1 + \hat{\sigma}_z)/2$ and $\hat{P}_1 = (1 - \hat{\sigma}_z)/2$ are projection operators of the system qubit. The first equation implies that physical bath-qubit decay can also transform into effective bath-spin excitation. It can therefore be active even when the bath is empty. Furthermore, this correlated noise wants to project the system spin to one of its $\hat{\sigma}_z$ eigenstates.

The effective Lindbladian becomes

$$\begin{aligned} \mathcal{L}_{\text{eff}}[\hat{\rho}] \approx & \frac{i}{\hbar} [\hat{\rho}, \hat{H}] + \gamma \sum_i \mathcal{L}_{\sigma_-^i}[\hat{\rho}] + \frac{\Gamma}{2} \sum_i \mathcal{L}_{\sigma_z^i}[\hat{\rho}] \\ & + \frac{\bar{\Gamma}}{2} \mathcal{L}_{\sigma_z}[\hat{\rho}]. \end{aligned} \quad (\text{B21})$$

where we have done noise factoring and neglected a contribution introducing bath excitation (this approximation was verified numerically). The size of $\bar{\Gamma}$ can also be solved numerically and gives a noticeable system-spin dephasing.

The effective noise analysis of a control-Z decomposition (defined later in Appendix C) is essentially the same as made for the CNOT-B decomposition, see Table II. This means that the effective noise of a control-Z decomposition has the same form as the physical noise.

Appendix C: Quantum circuit optimization

We assume that the effective noise given by \mathcal{L}_{eff} is dominated by spin damping and spin dephasing. As discussed above, this is possible for circuit decompositions based on native (small-angle) decompositions. However, if large-angle gates are needed, the quantum circuits should be designed so that the large angle gates act only on noiseless system qubits, or one uses large-angle gates that do not modify the noise. Also, the simulation algorithm used (like the SWAP algorithm) should ideally support this approach. Furthermore, if also the system qubits are noisy, it may be beneficial to transform the system noise to a symmetric form, in order to map it to an open-system model. These aspects are discussed in detail in this Appendix.

	$\sigma_-^{\text{control}}$	$\sigma_+^{\text{control}}$	$\sigma_z^{\text{control}}$	σ_-^{target}	σ_+^{target}	σ_z^{target}
CNOT	$\sigma_-^{\text{control}}\sigma_x^{\text{target}}$	$\sigma_+^{\text{control}}\sigma_x^{\text{target}}$	$\sigma_z^{\text{control}}$	$P_0\sigma_-^{\text{target}} + P_1\sigma_+^{\text{target}}$	$P_0\sigma_+^{\text{target}} + P_1\sigma_-^{\text{target}}$	$\sigma_z^{\text{control}}\sigma_z^{\text{target}}$
Control-Z	$\sigma_-^{\text{control}}\sigma_z^{\text{target}}$	$\sigma_+^{\text{control}}\sigma_z^{\text{target}}$	$\sigma_z^{\text{control}}$	$\sigma_-^{\text{target}}\sigma_z^{\text{control}}$	$\sigma_+^{\text{target}}\sigma_z^{\text{control}}$	σ_z^{target}

TABLE II: Effective noise for different incoming noise types and two-qubit gates. We consider physical noise operators $\hat{\sigma}_-$, $\hat{\sigma}_+$, $\hat{\sigma}_z$ under control-X (CNOT) and control-Z unitary transformations. Here $\hat{P}_0 = (1 + \hat{\sigma}_z^{\text{control}})/2$ and $\hat{P}_1 = (1 - \hat{\sigma}_z^{\text{control}})/2$ are control-qubit projection operators.

1. Avoiding large-angle bath-qubit rotations

Large-angle rotations of bath qubits may rotate the noise operators σ_+^i and σ_z^i to very different forms. Such rotations should then clearly be avoided. We give below several examples of gate decompositions that follow this principle.

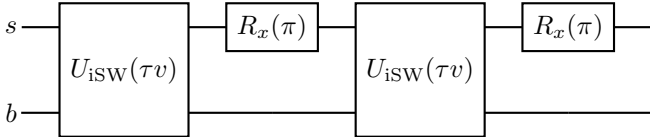
Ideally we have access to a native gate of some two-qubit interaction. In this paper we construct time-propagation according to XX-interaction between a system qubit and a bath qubit. Consider realizing this using a variable iSWAP two-qubit gate, which is a native gate of an excitation hop,

$$\hat{U}_{\text{iSWAP}}(\tau v) = e^{-i(\hat{\sigma}_+^s \hat{\sigma}_-^b + \hat{\sigma}_-^s \hat{\sigma}_+^b)\tau v/2}. \quad (\text{C1})$$

Here s refers to a system qubit and b to a bath qubit. To obtain the full XX-interaction, we need to add the counter-rotating terms. We can create these terms by another variable iSWAP gate by surrounding it by X-gates of one qubit. To avoid rotations of the bath qubit, the X-gates are applied to the system qubit,

$$\hat{R}_{x,s}(\pi)\hat{U}_{\text{iSWAP}}(\tau v)\hat{R}_{x,s}(\pi) = e^{-i(\hat{\sigma}_+^s \hat{\sigma}_-^b + \hat{\sigma}_-^s \hat{\sigma}_+^b)\tau v/2}. \quad (\text{C2})$$

The full XX-interaction time-propagation during one Trotter time step τ is then generated by



Here we marked $U_{\text{iSWAP}}(\tau v)$ by $U_{\text{iSW}}(\tau v)$. When using this construction, and assuming noiseless system qubits, the physical and effective noise Lindbladians have the same form. Note that this is not the case for the decomposition where X-gates are performed on the bath qubits.

On the other hand, to obtain an excitation hop using the native XX-gate

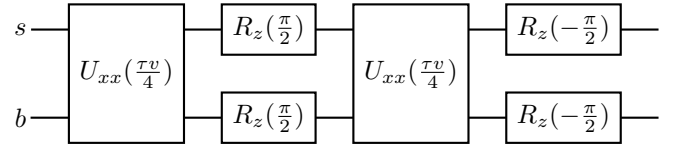
$$\hat{U}_{xx}(\tau v) = e^{-i\hat{\sigma}_x^s \hat{\sigma}_x^b \tau v/2}, \quad (\text{C3})$$

we need to supplement this with YY interaction. This can be created from an XX-gate with the help of Z-

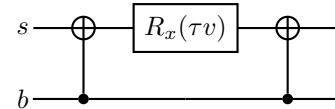
rotations,

$$\begin{aligned} & \hat{R}_{z,s} \left(-\frac{\pi}{2} \right) \hat{R}_{z,b} \left(-\frac{\pi}{2} \right) U_{xx}(\tau v) R_{z,b} \left(\frac{\pi}{2} \right) R_{z,s} \left(\frac{\pi}{2} \right) \\ & = e^{-i\hat{\sigma}_y^s \hat{\sigma}_y^b \tau v/2}. \end{aligned} \quad (\text{C4})$$

Note that this also includes large-angle rotations of the bath qubit. However, Z-rotations do not change the form of damping ($\hat{\sigma}_-$) or dephasing ($\hat{\sigma}_z$) operators (they just introduce a phase shift which cancels out in the Lindbladian). The excitation hop is then generated by

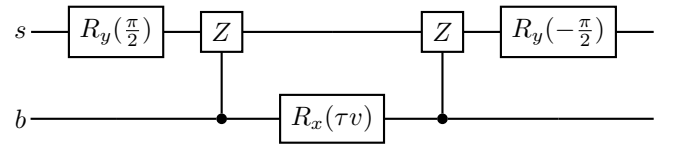


Also non-native two-qubit gate decompositions should follow this principle. For example, according to our results in the case of CNOT decomposition, using the bath qubit as a control-qubit seems beneficial. This can be understood qualitatively as a result of the fact that the bath qubit is never flipped (subjected to a large-angle gate). A non-native decomposition of the XX-interaction following these principles is



This is used in the CNOT-B decomposition of Sec. IV A. Here also notable is that the decomposition is not based on applying Hadamard-gates and small-angle Z-rotations, but instead uses direct small-angle X-rotations.

Another example of decomposing the XX-interaction using these principles is the control-Z decomposition



2. System-bath SWAP algorithm

In common open-system models the bath is non-interacting. For the presented quantum algorithm this

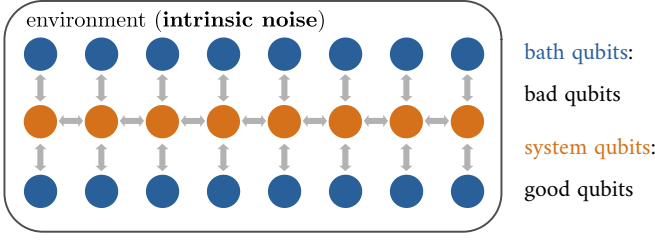
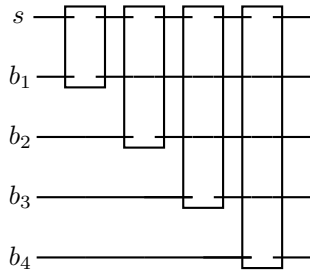
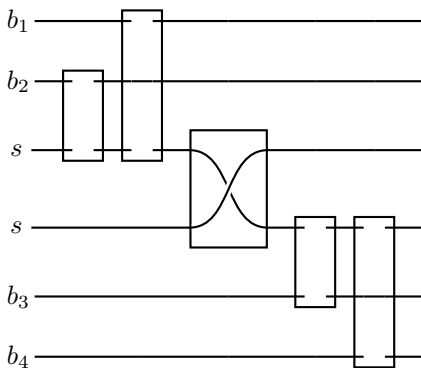


FIG. 8: A two-dimensional qubit architecture that is optimal for performing a Trotterized time evolution of a system-bath model. In total n_s system qubits locate between $2n_s$ bath qubits. The bath qubits can also refer to any other resonance modes in the device, whose interaction with the system qubits can be controlled digitally.

means that a direct connectivity between the bath qubits is not needed. Rather a connectivity from the system to all bath qubits (star geometry). If this is provided, a simple Trotter expansion of the time-propagation is adequate,



On the other hand, if only nearest-neighbor interactions are possible, but the device has a two-dimensional architecture, an efficient SWAP-algorithm can be applied. Our proposed system-bath SWAP algorithm converts the time evolution into a sequence of nearest-neighbor interactions and SWAP processes. Here the quantum state(s) of the system spin(s) are moved in a system-qubit network, located between the bath qubits, see Fig. 8. The difference to the common SWAP algorithm [48] is that bath states are not swapped. Within this modification, one avoids doing large-angle rotations of the bath qubits. In the example circuit below, the state of one system-spin is stored by two system qubits, one per time. The system spin interacts with four auxiliary spins, represented by the four bath qubits:



Note that this method most optimally time-propagates n_s system spins coupled to $2n_s$ auxiliary spins.

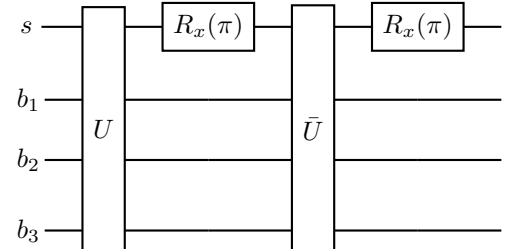
3. System-noise symmetrization

So far we have assumed that the system qubits are noiseless. Finite system noise may also be included, if it is transformed into the proper form. This is achieved by noise symmetrization, which in practice maps system noise to heating of the bath.

A simple example of noise symmetrization is the application of X-gates to transform physical qubit-damping into effective spin-excitation. This is based on the transformation

$$\hat{\sigma}_x \hat{\sigma}_- \hat{\sigma}_x = \hat{\sigma}_+ . \quad (\text{C5})$$

In the simplest version of the noise symmetrization, we insert X-gates between (original) Trotter-steps, and make corresponding changes to the unitary gates (such as $Y \rightarrow -Y$). In the case of system-qubit damping symmetrization, we then have the new Trotter-step circuits



where $\bar{U} = R_{x,s}(\pi) U R_{x,s}(\pi)$. Ideally the decomposition of U is similar to that of \bar{U} , or even $U = \bar{U}$ (which would be the case for an XX-interaction). This symmetrizes the effective Lindbladian \mathcal{L}_{eff} terms as

$$\gamma \hat{\sigma}_- \hat{\rho} \hat{\sigma}_+ \rightarrow \frac{\gamma}{2} \hat{\sigma}_- \hat{\rho} \hat{\sigma}_+ + \frac{\gamma}{2} \hat{\sigma}_+ \hat{\rho} \hat{\sigma}_- . \quad (\text{C6})$$

Furthermore, since

$$\frac{\gamma}{2} \hat{\sigma}_- \hat{\rho} \hat{\sigma}_+ + \frac{\gamma}{2} \hat{\sigma}_+ \hat{\rho} \hat{\sigma}_- = \frac{\gamma}{4} \hat{\sigma}_X \hat{\rho} \hat{\sigma}_X + \frac{\gamma}{4} \hat{\sigma}_Y \hat{\rho} \hat{\sigma}_Y , \quad (\text{C7})$$

we see that damping has changed to a coupling to two independent baths, via operators $\hat{\sigma}_x$ and $\hat{\sigma}_y$. As demonstrated in Sec. IV C and discussed more in Appendix E, this can be mapped to a constant background of spectral functions in a certain interesting class of open system models.

The system-noise symmetrization can be generalized to all spin-directions, in which case the system-noise becomes equivalent to depolarization. This corresponds to coupling to three independent baths, via operators $\hat{\sigma}_x$, $\hat{\sigma}_y$, and $\hat{\sigma}_z$. In fact, damping during X-gates may transform partly into $\hat{\sigma}_z$ -noise [22] in terms of the circuit-level noise that is inserted after the X-gates, in which case the bath mapping to $\hat{\sigma}_x$ and $\hat{\sigma}_y$ noise (shown above) is

approximate. In this case, it can be made exact when symmetrizing to full depolarization. Various noise symmetrization approaches have been studied experimentally in Refs. [12, 15].

Appendix D: Error sources and error tradeoff

Here we analyze three main error sources in the quantum algorithm and discuss how they are connected to each other. These are the Trotter error, the coarse-graining error, and the bath-Gaussianity error.

1. Trotter error

The time propagation is realized in time steps τ . Unless all terms in the Trotter expansion commute, there is an error in the time propagation. To have a small Trotter error, one commonly demands

$$v\tau \ll 1, \quad (\text{D1})$$

where v is some effective frequency describing the non-commuting contributions. This could be the system-bath coupling. One should note that even in situations where this relation is not always strictly valid, the Trotter error may still be small. In fact, in the examples we found that even values close to 1 may be tolerable.

The accumulation of noise within one Trotter-step circuit is also distributed, which implies that a similar error also exists in the effective noise model \mathcal{L}_{eff} . Assuming that the noise terms commute with each other, or that the noise has a smaller or similar magnitude as the coherent terms, the cautious estimate for the corrections to the noise model being small is

$$v\kappa\tau^2 \ll \kappa\tau, \quad (\text{D2})$$

This condition turns out to be equivalent to Eq. (D1).

In the mapping (Sec. III), the time step τ becomes related to the circuit depth D , the mode broadening κ , and the gate error ϵ , such that

$$\kappa\tau = D\epsilon, \quad (\text{D3})$$

The condition for the Trotter error and the noise-model error being small can now be rewritten as

$$D\epsilon \ll \frac{\kappa}{v}. \quad (\text{D4})$$

In the case $\kappa \approx v$, we get the simple relation

$$D\epsilon \ll 1. \quad (\text{D5})$$

The main message here is that the Trotter error is expected to decrease with the gate error ϵ . Moreover, for large ϵ , one may be forced to reduce the circuit depth D , which is practically done by reducing the total bath-qubit

number $n_q = \sum_{i=1}^n N_i$. Also notable is that a decrease in the broadening κ in comparison to v makes the condition more strict. The role of the broadening κ in the error analysis will be discussed more below.

2. Coarse-graining error and error correction

Unless the target spectral function is Lorentzian, or a (finite) sum of Lorentzians, there is always an error in the coarse graining. This error can be characterized, for example, by the root mean-square error of the spectral-function fit.

Several recent works study errors originating in the imperfect spectral-function fitting, as well as their correction, in the context of classical numerical methods [26, 49, 50]. Particularly interesting for the noise-utilizing quantum algorithm is an error-correction approach based on calculating functional derivatives with respect to spectral-function changes [26]. For the quantum algorithm considered here, this would correspond to using a low-noise qubit as a narrow-peak perturbation in the spectral function, to implement a functional derivative. The leading-order correction is the derivative multiplied by the coarse-graining error [26].

3. Error tradeoff

There is a close tradeoff between the different error sources. The coarse graining is always done within some frequency window, for example, within a cutoff frequency ω_c . In the simplest (yet still reasonably accurate) estimate, the auxiliary boson modes are inserted at constant frequency intervals with broadenings

$$\kappa \approx \frac{\omega_c}{n}. \quad (\text{D6})$$

We already note that an increase of n decreases κ . The circuit depth also depends on n and for the models considered in this paper it is approximately

$$D \approx nND_0 = n_q D_0, \quad (\text{D7})$$

where N is the number of qubits representing an auxiliary boson mode and for simplicity we assume that it is the same for every boson mode. The constant D_0 is defined by the simulation algorithm and the gate decomposition, see Table I.

Combining the above results with Eq. (D3) gives

$$\frac{\omega_c\tau}{\epsilon} \approx n^2ND_0. \quad (\text{D8})$$

On the left-hand side, the numerator $\omega_c\tau$ is a measure of the Trotter error. The denominator ϵ is a measure of the gate error. On the right-hand side, we have the number of Lorentzians used in the coarse graining n (also defining

the coarse-graining error) and the number of bath qubits per boson mode N .

Eq. (D8) implies that reducing the gate error ϵ allows us to increase n , N , or allows us to reduce the Trotter error $\omega_c\tau$. In other words, the lower the gate error ϵ , the better the quantum algorithm can perform. We also observe that higher gate errors can be compensated by increased Trotter error. Also notable is the fact that increasing the number of auxiliary boson modes n is challenging since its scaling is quadratic. This is since increasing n not only increases the circuit depth but also decreases κ .

Appendix E: Spin-boson model of electronic transport

In this Appendix, we discuss how to approximately map a fermionic open-system model to a spin-boson model. The key steps are (i) the assumption of Gaussian statistics of the fermion coupling operator, (ii) the replacement of this operator by a boson coupling operator, and (iii) the matching of the spectral functions. It should be noted that this procedure is not restricted to the specific Hamiltonian considered below but is also more generally applicable.

Our open quantum system is described by the Hamiltonian $\hat{H} = \hat{H}_S + \hat{H}_B + \hat{H}_C$, where

$$\hat{H}_S = \frac{\hbar\Delta}{2}\hat{\sigma}_z, \quad (\text{E1})$$

$$\hat{H}_B = \sum_m \sum_k E_{km} \hat{c}_{km}^\dagger \hat{c}_{km} + \sum_m \sum_l E_{lm} \hat{d}_{lm}^\dagger \hat{d}_{lm}, \quad (\text{E2})$$

$$\hat{H}_C = \hat{\sigma}_+ \hat{F} + \hat{\sigma}_- \hat{F}^\dagger, \quad (\text{E3})$$

where the fermion coupling operator is

$$\hat{F} = \sum_{klm} T_{klm} \hat{c}_{km}^\dagger \hat{d}_{lm}. \quad (\text{E4})$$

Here the operators $\hat{c}^{(\dagger)}$ and $\hat{d}^{(\dagger)}$ annihilate (create) an electron in the system and in the bath, correspondingly. Simultaneously, the state of the island spin is flipped. The transverse level m does not change in this electron transport event.

It has been understood that in the limit of a large number of transverse levels, the bath coupling operator \hat{F} becomes a Gaussian variable. Physically, in this limit, consecutive spin-flips which are induced by the system-bath electron hopping always involve electron transitions corresponding to separate transverse levels. On the Keldysh contour, this step is often referred to as the loop approximation, which is taken for example in Ref. [43] for metallic transistors. For systems with only one transverse channel instead, the loop approximation can be valid (at least) when the bath memory time is shorter than the average time between electron hoppings between the island and a lead.

When establishing the equivalent spin-boson model, a central role is played by the spectral function of the coupling operator \hat{F} ,

$$\begin{aligned} S(\omega) &= \left\langle \hat{F}^\dagger(t) \hat{F}(0) \right\rangle_\omega = \left\langle \hat{F}(t) \hat{F}^\dagger(0) \right\rangle_\omega \\ &= 2\pi \sum_m \sum_k \sum_l |T_{klm}|^2 \delta(\omega - E_{lm}/\hbar + E_{km}/\hbar) \\ &\quad \times f(E_{lm}) [1 - f(E_{km})], \end{aligned} \quad (\text{E5})$$

where $f(E)$ is the Fermi function and the index ω refers to a Fourier transformation under a free evolution of the bath, as in Eq. (A4). When writing down the corresponding spin-boson model, we also need to account for the fact that the coupling operator \hat{F} is not Hermitian and that the opposite-direction spin-flips are described by the same spectral function $S(\omega)$, see Eq. (E5). It follows that replacing \hat{F} by a boson position-operator $\hat{B} + \hat{B}^\dagger$, or by \hat{B} , is not satisfactory. A replacement of type

$$\hat{F} \rightarrow \hat{B}_1 + \hat{B}_2^\dagger. \quad (\text{E6})$$

where operators $\hat{B}_1^{(\dagger)}$ and $\hat{B}_2^{(\dagger)}$ are independent but characterized by a spectral function of the same form (see below), is found to be satisfactory. Since the free-evolution statistics of bosonic creation and annihilation operators are Gaussian, the two baths (fermionic and bosonic) are indistinguishable for an observer from the system, if the spectral functions match.

According to these observations, a spin-boson model that describes the original spin-fermion problem is of the form

$$\hat{H}_S = \frac{\hbar\Delta}{2}\hat{\sigma}_z, \quad (\text{E7})$$

$$\hat{H}_B = \sum_k \hbar\omega_k \hat{B}_{1k}^\dagger \hat{B}_{1k} + \sum_k \hbar\omega_k \hat{B}_{2k}^\dagger \hat{B}_{2k}, \quad (\text{E8})$$

$$\hat{H}_C = \hat{\sigma}_+ \sum_k v_k (\hat{B}_{1k} + \hat{B}_{2k}^\dagger) + \hat{\sigma}_- \sum_k v_k (\hat{B}_{1k}^\dagger + \hat{B}_{2k}). \quad (\text{E9})$$

A spin flip $\hat{\sigma}_+$ absorbs a boson from field 1 and creates a boson into field 2. The spectral function, in thermal equilibrium, is given by:

$$\begin{aligned} S(\omega) &= \sum_k \left\langle \hat{B}_{1k}^\dagger(t) \hat{B}_{1k}(0) \right\rangle_\omega + \sum_k \left\langle \hat{B}_{2k}^\dagger(t) \hat{B}_{2k}(0) \right\rangle_\omega \\ &= 2\pi \sum_k \frac{v_k^2 \delta(|\omega| - \omega_k)}{1 - \exp\left(-\frac{\hbar\omega}{k_B T}\right)} \text{sign}(\omega). \end{aligned} \quad (\text{E10})$$

The spin-boson model parameters v_k are chosen so that the spectral function of the fermionic problem is reproduced. In the example of Sec. IV C, we choose a struc-

tured spectral function of the form

$$S(\omega) = \sum_{k=0}^1 \frac{\alpha\omega}{1 - \exp\left(-\frac{\omega}{k_B T}\right)} \frac{1}{2\pi} \frac{\kappa'}{\left(\frac{\kappa'}{2}\right)^2 + (\omega - \omega_k)^2}, \quad (\text{E11})$$

where $\alpha = 0.25$, $\kappa' = 0.4\omega_0$, $\omega_1 = 2\omega_0$, and a cut-off function $1/[1 + (\omega/\omega_c)^4]$ with $\omega_c = \sqrt{3}\omega_0$. The spectral function $S(\omega)$ is then the target function in the coarse graining.

The form of coupling Hamiltonian (E9) supports the use of the variable iSWAP two-qubit decomposition, since it is the native gate of (system-bath) coupling $\hat{\sigma}_+ \hat{\sigma}_-^i + \hat{\sigma}_- \hat{\sigma}_+^i$. The counter-rotating coupling terms $\hat{\sigma}_+ \hat{\sigma}_+^i + \hat{\sigma}_- \hat{\sigma}_-^i$ can be created by surrounding the variable iSWAP by X-gates, see Appendix C.

Alternatively, an equivalent spin-boson Hamiltonian supporting the variable MS (native XX) decomposition can be derived by defining new bosonic operators

$$\hat{a}_k = \frac{1}{\sqrt{2}} (\hat{B}_{1k} + \hat{B}_{2k}) \quad (\text{E12})$$

$$\hat{b}_k = \frac{i}{\sqrt{2}} (-\hat{B}_{1k} + \hat{B}_{2k}). \quad (\text{E13})$$

This changes the form of the coupling Hamiltonian,

$$H_B = \sum_k \hbar\omega_k \hat{a}_k^\dagger \hat{a}_k + \sum_k \hbar\omega_k \hat{b}_k^\dagger \hat{b}_k, \quad (\text{E14})$$

$$H_C = \hat{\sigma}_x \sum_k \frac{v_k}{\sqrt{2}} (\hat{a}_k^\dagger + \hat{a}_k) + \hat{\sigma}_y \sum_k \frac{v_k}{\sqrt{2}} (\hat{b}_k^\dagger + \hat{b}_k). \quad (\text{E15})$$

When representing this with spin-spin Hamiltonian, the first coupling-term is replaced by $\hat{\sigma}_x \hat{\sigma}_x^i$ -interaction and the second coupling-term by $\hat{\sigma}_y \hat{\sigma}_x^i$ -interaction. The first coupling type is native to variable MS, whereas the second one can be created by surrounding the variable MS by $\pi/2$ Z-rotations, see Appendix C. It follows that the circuit depth, when time-propagating the system with variable MS according to this Hamiltonian, will be the same as when time-propagating the system with variable iSWAP according to the Hamiltonian (E9).

When time-evolving the open-system model on the quantum computer with a noisy system qubit, system-qubit X-gates are introduced between Trotter steps. This is done to transform physical system-qubit decay partly into effective excitation, see Appendix C. After this symmetrization, the physical decay noise corresponds to an effective noise that has equal contribution of system decay and excitation. Equivalently, the physical decay noise corresponds to an effective noise that has equal contribution of incoherent X-flips and Y-flips, see Eq. (C7). These system-environment coupling operators are the same as in the considered system-bath model. It follows that system noise can be mapped to a constant background of the bath the spectral functions, see Sec. III A 2 and Eq. (11). This mapping is demonstrated in practice in the example of Sec. IV C.

[1] I. M. Georgescu, S. Ashhab, and F. Nori, Rev. Mod. Phys. **86**, 153 (2014), URL <https://doi.org/10.1103/RevModPhys.86.153>.

[2] K. Bharti, A. Cervera-Lierta, T. H. Kyaw, T. Haug, S. Alperin-Lea, A. Anand, M. Degroote, H. Heimonen, J. S. Kottmann, T. Menke, et al., Rev. Mod. Phys. **94**, 015004 (2022), URL <https://doi.org/10.1103/RevModPhys.94.015004>.

[3] H.-P. Breuer and F. Petruccione, *The Theory of Open Quantum Systems* (Oxford University Press on Demand, Oxford, 2002).

[4] H. Weimer, A. Kshetrimayum, and R. Orús, Rev. Mod. Phys. **93**, 015008 (2021), URL <https://doi.org/10.1103/RevModPhys.93.015008>.

[5] A. Ishizaki and G. R. Fleming, Annu. Rev. Condens. Matter Phys. **3**, 333 (2012), URL <https://doi.org/10.1146/annurev-conmatphys-020911-125126>.

[6] A. J. Leggett, S. Chakravarty, A. T. Dorsey, M. P. A. Fisher, A. Garg, and W. Zwerger, Rev. Mod. Phys. **59**, 1 (1987), URL <http://dx.doi.org/10.1103/RevModPhys.59.1>.

[7] S. Lloyd and L. Viola, Phys. Rev. A **65**, 010101(R) (2001), URL <https://doi.org/10.1103/PhysRevA.65.010101>.

[8] H. Wang, S. Ashhab, and F. Nori, Phys. Rev. A **83**, 062317 (2011), URL <https://doi.org/10.1103/PhysRevA.83.062317>.

[9] G. García-Pérez, M. A. C. Rossi, and S. Maniscalco, npj Quantum Inf. **6**, 1 (2020), URL <https://doi.org/10.1038/s41534-019-0235-y>.

[10] K. Head-Marsden, S. Krastanov, D. A. Mazzotti, and N. P., Phys. Rev. Research **3**, 013182 (2021), URL <https://doi.org/10.1103/PhysRevResearch.3.013182>.

[11] J. T. Barreiro, M. Müller, P. Schindler, D. Nigg, T. Monz, M. Chwalla, M. Hennrich, C. F. Roos, P. Zoller, and R. Blatt, Nature **470**, 486 (2011), URL <https://doi.org/10.1038/nature09801>.

[12] B. Rost, B. Jones, M. Vyushkova, A. Ali, C. Cullip, A. Vyushkov, and J. Nabrzyski, arXiv:2001.00794 (2020), URL <https://arxiv.org/abs/2001.00794>.

[13] B. Rost, L. Del Re, N. Earnest, A. F. Kemper, B. Jones, and J. K. Freericks, arXiv:2108.01183 (2021), URL <https://arxiv.org/abs/2108.01183>.

[14] J. Han, W. Cai, L. Hu, X. Mu, Y. Ma, Y. Xu, W. Wang, H. Wang, Y. P. Song, C.-L. Zou, et al., Phys. Rev. Lett.

127, 020504 (2021), URL <https://doi.org/10.1103/PhysRevLett.127.020504>.

[15] S. Sun, L.-C. Shih, and Y.-C. Cheng, arXiv.2106.12882 (2021), URL <https://doi.org/10.48550/arXiv.2106.12882>.

[16] Z. Hu, K. Head-Marsden, D. A. Mazziotti, P. Narang, and S. Kais, *Quantum* **6**, 726 (2022), URL <https://doi.org/10.22331/q-2022-05-30-726>.

[17] N. Suri, J. Barreto, S. Hadfield, N. Wiebe, F. Wudarski, and J. Marshall, arXiv.2207.10007 (2022), URL <https://doi.org/10.48550/arXiv.2207.10007>.

[18] H. Kamakari, S.-N. Sun, M. Motta, and A. J. Minnich, *PRX Quantum* **3**, 010320 (2022), URL <http://dx.doi.org/10.1103/PRXQuantum.3.010320>.

[19] S. Lloyd, *Science* **273**, 1073 (1996), URL <https://doi.org/10.1126/science.273.5278.1073>.

[20] C. H. Tseng, S. Somaroo, Y. Sharf, E. Knill, R. Laflamme, T. F. Havel, and D. G. Cory, *Phys. Rev. A* **62**, 032309 (2000), URL <https://doi.org/10.1103/PhysRevA.62.032309>.

[21] E. Zapusek, A. Javadi, and F. Reiter, *Quantum Sci. Technol.* **8**, 015001 (2022), URL <https://doi.org/10.1088/2058-9565/ac98dd>.

[22] K. R. Fratus, K. Bark, N. Vogt, J. Leppäkangas, S. Zanker, M. Marthaler, and J.-M. Reiner, arXiv.2210.11371 (2022), URL <https://doi.org/10.48550/arXiv.2210.11371>.

[23] F. Arute, K. Arya, R. Babbush, D. Bacon, J. C. Bardin, R. Barends, A. Bengtsson, S. Boixo, M. Broughton, B. B. Buckley, et al., arXiv.2010.07965 (2020), URL <https://doi.org/10.48550/arXiv.2010.07965>.

[24] J. Leppäkangas, J. Braumüller, M. Hauck, J.-M. Reiner, I. Schwenk, S. Zanker, L. Fritz, A. V. Ustinov, M. Weides, and M. Marthaler, *Phys. Rev. A* **97**, 052321 (2018), URL <http://dx.doi.org/10.1103/PhysRevA.97.052321>.

[25] E. Arrigoni, M. Knap, and W. von der Linden, *Phys. Rev. Lett.* **110**, 086403 (2013), URL <https://doi.org/10.1103/PhysRevLett.110.086403>.

[26] A. Dorda, M. Nuss, W. von der Linden, and E. Arrigoni, *Phys. Rev. B* **89**, 165105 (2014), URL <https://doi.org/10.1103/PhysRevB.89.165105>.

[27] D. Tamaselli, A. Smirne, S. F. Huelga, and M. B. Plenio, *Phys. Rev. Lett.* **120**, 030402 (2018), URL <http://dx.doi.org/10.1103/PhysRevLett.120.030402>.

[28] F. Chen, E. Arrigoni, and M. Galperin, *New J. Phys.* **21**, 123035 (2019), URL <http://dx.doi.org/10.1088/1367-2630/ab5ec5>.

[29] G. Pleasance, B. M. Garraway, and F. Petruccione, *Phys. Rev. Research* **2**, 043058 (2020), URL <http://dx.doi.org/10.1103/PhysRevResearch.2.043058>.

[30] G. Pleasance and F. Petruccione, arXiv:2108.05755 (2021), URL <https://arxiv.org/abs/2108.05755>.

[31] S. Mostame, P. Rebentrost, A. Eisfeld, A. J. Kerman, D. I. Tsomokos, and A. Aspuru-Guzik, *New J. Phys.* **14**, 105013 (2012), URL <https://doi.org/10.1088/1367-2630/14/10/105013>.

[32] A. Lemmer, C. Cormick, D. Tamaselli, T. Schaetz, S. F. Huelga, and M. B. Plenio, *New J. Phys.* **20**, 073002 (2018), URL <https://doi.org/10.1088/1367-2630/aac87d>.

[33] A. Potočnik, A. Bargerbos, F. A. Y. N. Schröder, S. A. Khan, M. C. Collodo, S. Gasparinetti, Y. Salathé, C. Creatore, C. Eichler, H. E. Türeci, et al., *Nature Communications* **9**, 904 (2018), URL <http://dx.doi.org/10.1038/s41467-018-03312-x>.

[34] B. M. Garraway, *Phys. Rev. A* **55**, 2290 (1997), URL <https://doi.org/10.1103/PhysRevA.55.2290>.

[35] A. Ishizaki and Y. Tanimura, *J. Phys. Soc. Jpn* **74**, 3131 (2005), URL <https://doi.org/10.1143/JPSJ.74.3131>.

[36] N. Lambert, S. Ahmed, M. Cirio, and F. Nori, *Nature Communications* **10**, 3721 (2019), URL <http://dx.doi.org/10.1038/s41467-019-11656-1>.

[37] N. P. D. Sawaya, T. Menke, T. H. Kyaw, S. Johri, A. Aspuru-Guzik, and G. G. Guerreschi, *npj Quantum Information* **6**, 49 (2020), URL <http://dx.doi.org/10.1038/s41534-020-0278-0>.

[38] F. Arute, K. Arya, R. Babbush, D. Bacon, J. C. Bardin, R. Barends, R. Biswas, S. Boixo, F. G. S. L. Bradao, D. A. Buell, et al., arXiv.1910.11333 (2019), URL <https://doi.org/10.48550/arXiv.1910.11333>.

[39] T. Abad, J. Fernández-Pendás, A. Frisk Kockum, and G. Johansson, *Phys. Rev. Lett.* **129**, 150504 (2022), URL <https://doi.org/10.1103/PhysRevLett.129.150504>.

[40] N. Vogt, K. Bark, M. Walt, S. Zanker, J.-M. Reiner, and M. Lodi, *qoqo*, URL <https://github.com/HQSQuantumSimulations/qoqo>.

[41] *QuEST – Quantum Exact Simulation Toolkit*, URL <https://quest.qtechtheory.org/>.

[42] L. Magazzù, P. Forn-Díaz, R. Belyansky, J.-L. Orgiazzi, M. A. Yurtalan, M. R. Otto, A. Lupascu, C. M. Wilson, and M. Grifoni, *Nat. Commun.* **9**, 1403 (2018), URL <http://dx.doi.org/10.1038/s41467-018-03626-w>.

[43] H. Schoeller and G. Schön, *Phys. Rev. B* **50**, 18436 (1994), URL <https://doi.org/10.1103/PhysRevB.50.18436>.

[44] S. E. Smart, Z. Hu, S. Kais, and D. A. Mazziotti, *Commun. Phys.* **5**, 28 (2022), URL <https://doi.org/10.1038/s42005-022-00803-8>.

[45] K. Wang, F. Piazza, and D. J. Luitz, *Phys. Rev. Lett.* **124**, 100604 (2020), URL <http://dx.doi.org/10.1103/PhysRevLett.124.100604>.

[46] O. E. Sommer, F. Piazza, and D. J. Luitz, *Phys. Rev. Research* **3**, 023190 (2021), URL <https://doi.org/10.1103/PhysRevResearch.3.023190>.

[47] J.-M. Reiner, S. Zanker, I. Schwenk, J. Leppäkangas, F. Wilhelm-Mauch, G. Schön, and M. Marthaler, *Quantum Sci. Technol.* **3**, 045008 (2018), URL <https://doi.org/10.1088/2058-9565/aad5ba>.

[48] I. D. Kivlichan, J. McClean, N. Wiebe, C. Gidney, A. Aspuru-Guzik, G. Kin-Lic Chan, and R. Babbush, *Phys. Rev. Lett.* **120**, 110501 (2018), URL <https://doi.org/10.1103/PhysRevLett.120.110501>.

[49] F. Mascherpa, A. Smirne, S. F. Huelga, and M. B. Plenio, *Phys. Rev. Lett.* **118**, 100401 (2017), URL <https://doi.org/10.1103/PhysRevLett.118.100401>.

[50] F. Mascherpa, A. Smirne, A. D. Somoza, P. Fernández-Acebal, S. Donadi, D. Tamaselli, S. F. Huelga, and M. B. Plenio, *Phys. Rev. A* **101**, 052108 (2020), URL <https://doi.org/10.1103/PhysRevA.101.052108>.